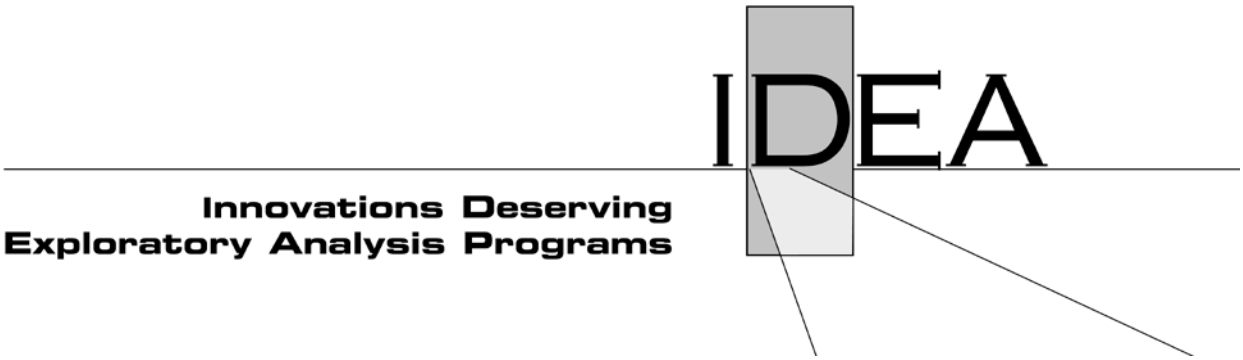

NCHRP IDEA Program

Drained Timber Pile Ground Improvement for Liquefaction Mitigation

Final Report for
NCHRP IDEA Project 180

Prepared by:
Armin W. Stuedlein and Tygh Gianella
Oregon State University

January 2016

TRB TRANSPORTATION RESEARCH BOARD
The National Academies of
SCIENCES · ENGINEERING · MEDICINE

Innovations Deserving Exploratory Analysis (IDEA) Programs Managed by the Transportation Research Board

This IDEA project was funded by the NCHRP IDEA Program.

The TRB currently manages the following three IDEA programs:

- The NCHRP IDEA Program, which focuses on advances in the design, construction, and maintenance of highway systems, is funded by American Association of State Highway and Transportation Officials (AASHTO) as part of the National Cooperative Highway Research Program (NCHRP).
- The Safety IDEA Program currently focuses on innovative approaches for improving railroad safety or performance. The program is currently funded by the Federal Railroad Administration (FRA). The program was previously jointly funded by the Federal Motor Carrier Safety Administration (FMCSA) and the FRA.
- The Transit IDEA Program, which supports development and testing of innovative concepts and methods for advancing transit practice, is funded by the Federal Transit Administration (FTA) as part of the Transit Cooperative Research Program (TCRP).

Management of the three IDEA programs is coordinated to promote the development and testing of innovative concepts, methods, and technologies.

For information on the IDEA programs, check the IDEA website (www.trb.org/idea). For questions, contact the IDEA programs office by telephone at (202) 334-3310.

IDEA Programs
Transportation Research Board
500 Fifth Street, NW
Washington, DC 20001

Drained Timber Pile Ground Improvement for Liquefaction Mitigation

IDEA Program Final Report

NCHRP 180

Prepared for the IDEA Program
Transportation Research Board
The National Academies

Armin W. Stuedlein, Ph.D., P.E.
Principal Investigator

and

Tygh Gianella
Graduate Research Assistant

School of Civil and Construction Engineering
Oregon State University
Corvallis, OR 97331

Date Submitted
January 2016

ACKNOWLEDGMENTS

Funding for this study was provided by the National Academy of Sciences through the National Cooperative Highway Research Program: Ideas Deserving Exploratory Analysis (NCHRP IDEA) Program under Project Number 180. This support is gratefully acknowledged.

The investigators would like to extend thanks to the members of the South Carolina Chapter of the Pile Driving Contractors Association (PDCA). We wish to thank Van Hogan, formerly of the PDCA, for his hard work and dedication in marshalling the various resources required to bring this project to completion. We thank the member firms that have contributed materials, labor, and equipment, and without whom this project could not have been completed: Pile Drivers, Inc.; S&ME, Inc.; Soil Consultants Inc.; Chuck Dawley Surveying; Cox Wood Industries; and Hayward Baker, Inc.

We also recognize and thank the members of the Expert Review Panel, whose comments have served to help guide this work. The authors thank Scott Ashford, Billy Camp, Joe Horton, Bernie Kleutsch, Silas Nichols, and Jeff Sizemore.

The conclusions developed from this study are those of the investigators and do not necessarily reflect the views of the sponsors.

TABLE OF CONTENTS

EXECUTIVE SUMMARY 1

1.0 IDEA PRODUCT 2

2.0 CONCEPT AND INNOVATION 2

3.0 INVESTIGATION 3

3.1 Investigation of Prototype Suitability 4

3.2 Subsurface Characterization Oof the Test Site 6

3.2.1 Geological Setting 6

3.2.2 Subsurface Conditions 6

3.2.3 Laboratory Test Analyses 9

3.2.4 Finalized Subsurface Model 12

3.3 Effect of Pile Spacing, Drainage, and Time on Densification 13

3.3.1 Test Pile Program 13

3.3.2 Evaluation of Pile Spacing on Densification 17

3.3.3 Effect of Drainage and Time 23

3.4 Controlled Blasting to Evaluate Pore Pressure Response and Post-Blasting Settlement 28

3.4.1 Experimental Details for the Controlled Blasting Program 299

3.4.2 Controlled Blasting of the Control Zone 30

3.4.3 Post-blasting Settlement of the Control Zone 33

3.4.4 Controlled Blasting of the Treated Zones 35

3.4.5 Post-blasting Settlement of the Treated Zones 37

3.5 Numerical Simulation of Controlled Blasting and Dissipation of Excess Pore Pressures 39

3.5.1 Numerical Simulation of the Control Zone 39

3.5.2 Numerical Simulation of the Treated Zones 40

4.0 PLANS FOR IMPLEMENTATION 46

4.1 Summary of Findings and Possible Improvements 46

4.2 Implementation of Findings 47

4.2.1 Considerations for Implementations 47

4.2.2 Technology Transfer 47

4.2.3 Demonstration Project 48

4.3 Closing Statement 48

5.0 REFERENCES 49

APPENDIX A NUMERICAL ANALYSES A-1

EXECUTIVE SUMMARY

Excess porewater pressure induced by rapid shearing often leads to liquefaction of granular deposits, resulting in excessive deformation (settlement, lateral spreading) and loss of stability of supported structures. Since several devastating earthquakes in the 1960s, practitioners and researchers have developed and evaluated numerous approaches for the mitigation of liquefaction and its deleterious effects on civil infrastructure. Innovations include vibro-compaction and vibro-replacement of granular deposits, compaction and permeation grouting, deep soil mixing and jet grouting, and installation of large-diameter, high-density polypropylene (HDPE) earthquake drains (EQDs). These mitigation techniques attempt to improve the ground such that the soil is densified, reinforced, or drained, lowering the potential for excessive ground deformation. Although the foregoing mitigation techniques enjoy strong theoretical and empirical evidence of their effectiveness, each of the methods exhibits the limitation that they use one mode of treatment (densification, reinforcement, or drainage). To overcome these limitations, the effectiveness of conventional and novel drained timber pile ground improvement for the mitigation of liquefaction was evaluated.

The results of this study showed that drained and conventional piles could effectively densify liquefiable soils, with increases in relative density ranging from 60 to 95 percent immediately following installation of timber piles, depending on the pile spacing and use of pre-fabricated vertical drains (PVDs). Long-term measurements of corrected cone tip resistance showed increases of approximately 30 percent for piles spaced at four to five diameters, *D*, with and without PVDs, 125 percent for piles at 3*D* without PVDs, and about 145 percent for piles spaced at 3*D* with drains and 2*D* without drains. Closely-spaced drained piles produced larger improvements in cone tip resistance than conventional piles at the same spacing (i.e., 3*D*). Controlled blasting of the timber pile treated areas showed that the treated soils responded in a dilative manner, resulting in decreases in excess pore pressure relative to an unimproved zone, and resulting in significantly smaller vertical ground deformations. Although areas for improvement in the drained pile prototype were identified, *there are no barriers to the immediate implementation of drained and/or conventional, driven timber displacement piles*. Because there is no proprietary information associated with this innovation, state departments of transportation and their design consultants may begin to implement this technology immediately.

1.0 IDEA PRODUCT

The product of this IDEA project is a ground improvement technology that joins two existing technologies currently available in the marketplace that are not being frequently used to mitigate liquefaction. The product evaluated herein is a pile fitted with drainage elements that, under sufficient conditions, serves to increase the tendency of soil to densify during pile driving, resulting in improved densification and resistance to cyclic shear stresses that are generated during earthquakes. The development and evaluation of this technology serves to provide the owners of public and private civil infrastructure with another alternative for surviving strong ground motion and its effects.

2.0 CONCEPT AND INNOVATION

Excess porewater pressure induced by rapid shearing often leads to the short-term loss of soil strength in contractive soils such as loose to medium dense coarse-grained (sands) and soft to medium stiff non-plastic fine-grained soils (silts and sandy silts). Development of excess porewater pressure can lead to delayed construction schedules in fine-grained soils and loss of global stability, particularly in bridge approach embankments (Figure 2.1). Earthquake-induced excess porewater pressure can lead to liquefaction of granular deposits, resulting in excessive deformation (settlement, lateral spreading) and loss of stability of supported structures. Since the 1964 M7.6 Niigata, Japan, and the M9.2 Good Friday, Alaska earthquakes, practitioners and researchers have developed and evaluated numerous approaches for the mitigation of liquefaction and its deleterious effects on civil infrastructure. Innovations range from vibro-compaction and vibro-replacement of granular deposits, compaction and permeation grouting, deep soil mixing and jet grouting, and installation of large-diameter high-density polypropylene (HDPE) earthquake drains (EQDs). These mitigation techniques attempt to improve the ground such that the soil is densified, reinforced, or drained, lowering the potential for excessive ground deformation. The aim of densification is to directly raise the cyclic resistance of the soil by changing the state of the soil structure from contractive to dilative. The goal of reinforcement is to provide stiffened elements within the sheared mass, diverting cyclic stresses from the liquefiable soil to the stiffer elements. Drainage provides a direct means to remove the de-stabilizing positive excess pore pressure from the sheared mass.

Although the foregoing mitigation techniques enjoy strong theoretical and empirical evidence of their effectiveness, each of the methods exhibits the limitation that they use one mode of treatment (densification, reinforcement, or drainage). The one technology that provides two potential modes of treatment, vibro-replacement, is subject to contamination of the open soil pore network with silty fines during construction, significantly reducing the drainage capacity of the granular column. Occasionally, two or more techniques are used to achieve the project schedule, such as the combined use of vibro-replacement stone columns and pre-fabricated vertical drains (PVDs) to accelerate densification by drainage, an inefficient and an added construction cost. Considerably under-utilized, timber piles can be used as a renewable ground improvement alternative, providing shear reinforcement and resulting in densification as the

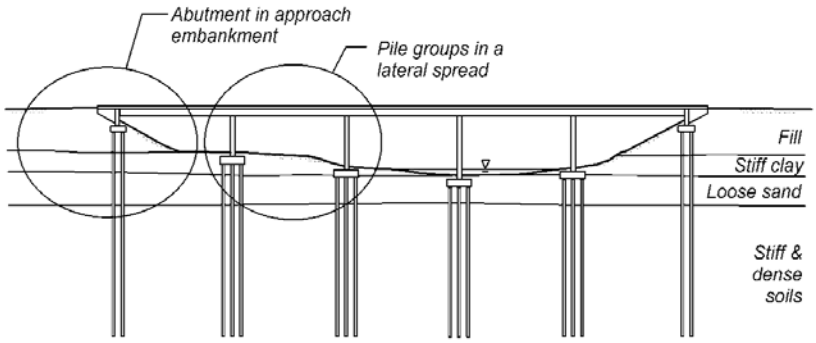

FIGURE 2.1 Typical cross section of bridge site showing two sub-systems requiring analyses of (1) pile groups in lateral spreading ground (developing due to soil liquefaction), and (2) pile-supported abutment in approach fill with potential global instabilities due to either construction or seismically induced (liquefaction) excess pore pressures (after Ashford et al. 2011).

installation of these solid cross-section elements cause a decrease in soil void space. By placing functional drains directly within this stiffened ground improvement alternative, the protection against seismically induced excess pore pressures and softening of the surrounding soil can be efficiently mitigated, resulting in a large envelope of drained soil. The result is an improved resistance to strong ground motion and liquefaction by virtue of the three-pronged approach to mitigation: densification, shear reinforcement, and drainage. This study was conducted to evaluate the effectiveness of conventional and drained timber pile ground improvement to mitigate soil liquefaction. This alternative could also be easily combined with a column-supported embankment concept as another added benefit.

3.0 INVESTIGATION

The purpose of this study is to investigate the effect of pile spacing, time elapsed since installation, and drainage on the amount of soil densification, and to compare the effectiveness of drained timber piles in mitigating liquefaction to that of conventional timber piles. The following tasks were conducted over the course of the study to meet the proposed objectives:

1. **Task 1**: Development of a drained timber pile prototype and the assessment of installation.
2. **Task 2**: Characterization of a suitable test site for full-scale evaluation of the selected timber pile prototypes and conventional timber piling.
3. **Task 3**: Investigation of the effect of timber pile spacing, drainage, and post-installation duration on driving-induced densification of liquefiable soils.
4. **Task 4**: Evaluation of effect of timber pile spacing and drainage on the reduction of excess pore pressures using blast liquefaction techniques.
5. **Task 5**: Evaluation of the effectiveness of existing analytical methods and software to predict the reduction in seismically induced excess pore pressures.

3.1 Investigation of Prototype Suitability

The goal of Task 1 was to evaluate the prototype drainage pile with a view to preventing installation damage to the drain. The shear strength of the drain material and its connection to the pile must be sufficient to resist the shear stresses along the soil-pile interface. The first drained pile prototype was generated by wrapping PVDs around the tip of the timber pile and attaching them along the length of the pile using roofing nail fasteners as shown in Figure 3.1. As shown in Figure 3.2 and summarized in Table 3.1, the PVDs consisted of high-discharge polypropylene core channels wrapped with non-woven geotextile fabric to prevent clogging of drains. The drain buckled during driving of the first test piles, as shown in Figure 3.3. When the pile was subsequently extracted, it was concluded that the pile hit debris and waste from Hurricane Hugo (1989) buried in the fill comprising the upper layer of soil. The debris cut into the PVD and timber, severing the PVD (Figure 3.4). A second prototype was constructed by doubling the number of fasteners along the pile shaft, and tripling the number of fasteners near the base of the pile (Figure 3.5). Additionally, each pile location was conditioned by pre-drilling 2 to 3 m in depth, and spudding through the debris when the augers encountered refusal. This approach was suggested by the pile driving contractor, who stated that pre-drilling was common for construction in South Carolina, and therefore this approach would fall within normal construction operations without inducing significant additional cost. The drained piles were driven without further problems, and this procedure and prototype was followed for all subsequent further pile installation (Figure 3.6).

FIGURE 3.1 Drained timber pile prototype with one fastener per 0.3 m (12 in.).

FIGURE 3.2 Pre-fabricated vertical drain (PVD) element.

FIGURE 3.3 First pile prototype during installation during buckling of PVD.

FIGURE 3.4 Damaged PVD and timber pile prototype.

FIGURE 3.5 Second pile prototype with additional fasteners.

FIGURE 3.6 Installation of second pile prototype within pre-drilled cavity.

Table 3.1. Mebra-Drain MD-88 specifications (from Hayward Baker 2014)

Drain Properties	
Core width (mm)	98
Core thickness (mm)	3.4
Total width (mm)	100
Total thickness (mm)	4.34
Permittivity (sec^{-1})	0.3
Apparent opening size (mm)	0.090
Discharge capacity @ 10 kPa (m^3/s)	1.57×10^{-4}
Discharge capacity @ 240 kPa (m^3/s)	1.44×10^{-4}

3.2 Subsurface Characterization of the Test Site

3.2.1 Geological Setting

The test site is located in Hollywood, South Carolina, adjacent to Highway 17, approximately 21 kilometers west of Charleston and 19 kilometers north of the coast line, as shown in Figure 3.7. This location is part of the Coastal Plain Unit, comprising marine and fluvial deposits, and covers approximately two-thirds of the state of South Carolina (SCDOT 2008). The Coastal Plain Unit consists of scarps and terraces as a result of the sea level rising and falling, resulting in interbedded layers of silts, sands, and clays (Doar and Kendall 2014). This action results in formations that are adjacent to one another rather than stacked vertically, with decreasing elevation as the plains approach the sea. According to the geologic map of South Carolina (Figure 3.8), the Lower Coastal Plain consists of Pleistocene-aged deposits (i.e., deposited 10,000 to 1.8 million years ago). Andrus et al. (2008) estimated that the sands in Hollywood, South Carolina, were approximately 200,000 years old using in situ tests.

FIGURE 3.7 Location of test site in Hollywood, South Carolina, USA (from USGS National Map Viewer).

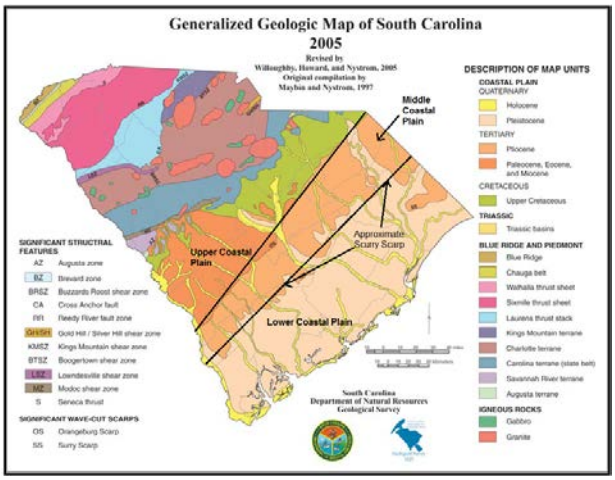

FIGURE 3.8 Geologic map with approximate plain locations (SCDOT 2008).

3.2.2 Subsurface Conditions

To establish the pre-installation stratigraphy and relative density of the test site, several explorations with and without soil sampling were required. The number and distribution of explorations were selected on the basis of pile spacing in the treated zones, which are described in detail in Section 3.3. Figure 3.9 shows a plan view of the test area indicating the general situation of the treated and control zones in the site. The area of the site where the piles were driven is a relatively flat, grassy area with dimensions of approximately 30 m by 7.5 m. Standard penetration tests (SPTs), cone penetration

tests (CPTs), and shear wave velocity tests were performed in Zones 1 through 5 and in the control zone to characterize the subsurface.

The first round of CPTs (i.e., prior to pile installation) was performed at pile locations 1, 6, 7, 8, and 9 near the center of each zone as shown in Figure 3.10. One seismic CPT (SCPT) was performed at the future location of Pile 1 in the center of each of the five zones to establish the downhole shear wave velocity for each zone. Exploratory borings with split spoon sampling were performed between Piles 3 and 7 in each zone. An exploratory boring and CPT was also performed at the Control Zone, which was located approximately 15 m northeast of Zone 5.

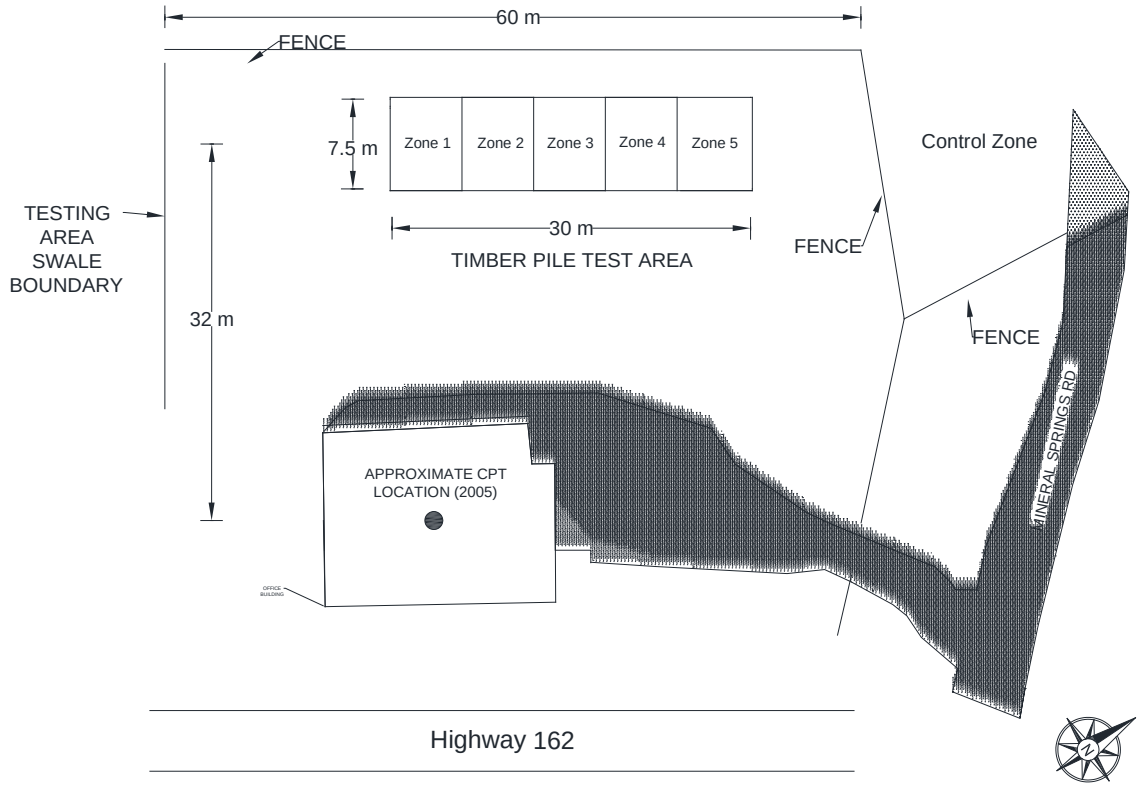

FIGURE 3.9 General layout of the test site indicating the location of the timber pile test area (Zones 1–5) and the control zone.

Corrected cone tip resistance, q_t, and SPT N_{60} blow counts from explorations located at the centers of Zones 1 through 5 and the Control Zone are shown in Figure 3.11, and represent a simplified cross section of the test site. Cone tip resistance measurements were corrected to account for the unequal pore pressures that act on the tip of the cone penetrometer using the procedure outlined in Mayne (2007). In general, the q_t and SPT N_{60} was relatively uniform across the site, and ranged between approximately 1 and 10 MPa and 1 and 10 blows per foot, respectively, to a depth of approximately 12.5 m. At this depth, the cone tip and standard penetration resistance increased sharply, indicating a contact with a dense soil layer. The characterization of the soil and stratigraphy of the test site was informed by an

extensive laboratory test program discussed in Section 3.2.3, and compiled to generate the representative subsurface model in Section 3.2.4, as described subsequently.

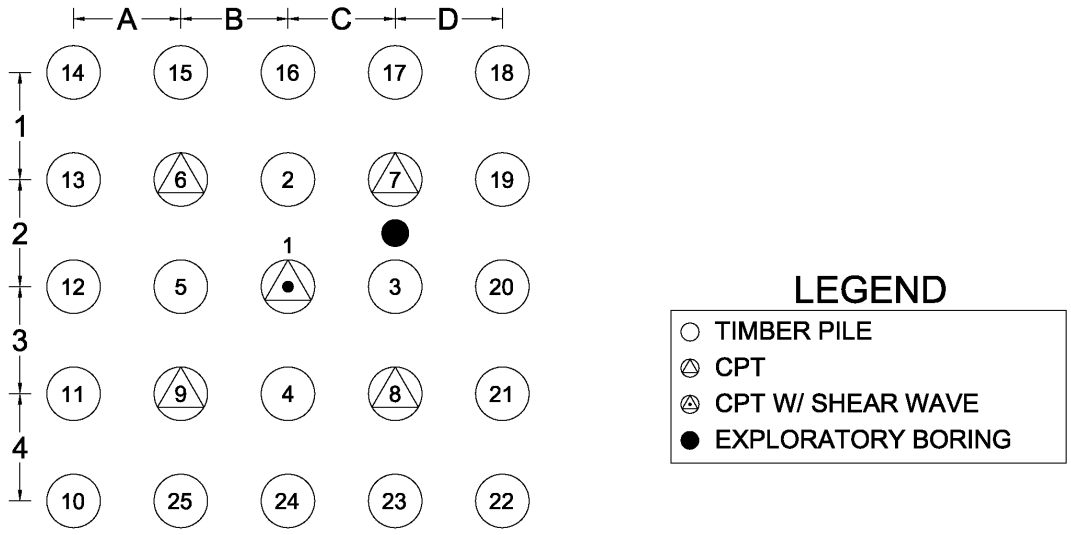

FIGURE 3.10. Location of pre-installation in situ tests for Zones 1–5.

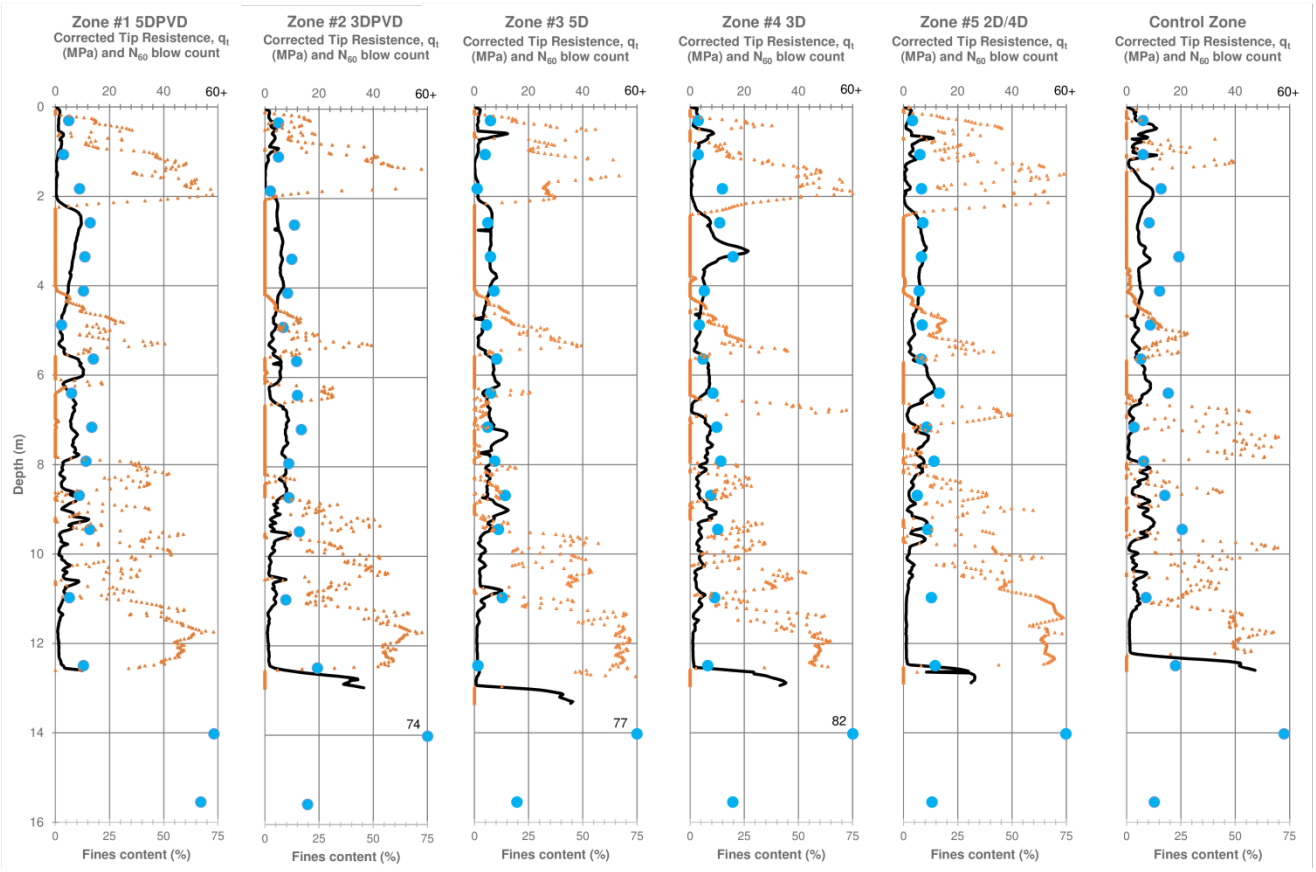

FIGURE 3.11. Baseline in situ tests results including SPT (blue markers) and CPT (black line), with calibrated fines content correlation (orange markers) results.

3.2.3 Laboratory Test Analyses

The standard penetration tests were performed by Soil Consultants Inc., and split-spoon samples were shipped to the geotechnical laboratory at Oregon State University, Corvallis, Oregon, for laboratory classification and testing. Samples were obtained at increments of approximately 0.75 m from 0.30 to 9.45 m below the ground surface and at increments of approximately 1.5 m from 9.45 to 15.5 m below the ground surface. Laboratory tests performed to characterize the soils and their susceptibility to liquefaction included: grain size distributions, #200 sieve (fines) washes, specific gravity, minimum and maximum void ratio tests, and Atterberg Limits. Additionally, microscopic images were obtained for the sand-size particles and their roundness and sphericity determined. Figure 3.12 below shows grain size distributions of samples from approximately 2.5 to 10.5 m below ground surface, corresponding to the liquefaction-susceptible soils. These soils are classified as a poorly graded, sub-rounded to rounded fine sand (SP) to silty fine sand (SP-SM). The soil is relatively clean, (i.e., fines content ranging from 1 to 10 percent) with occasional lenses of silty sand, for depths of approximately 2.5 and 10.5 m below the ground surface. Additional details regarding the laboratory test program are described in Gianella (2015).

After evaluation of several correlations of SPT-*N*, subsurface data, and cone tip resistance to relative density, D_r, the correlation developed by Mayne (2007) was selected as producing the most representative CPT-based estimate. The Mayne (2007) correlation to D_r is given by:

$$D_r(\%) = 100\left[0.268\ln\left(\frac{q_t/\sigma_{atm}}{\sqrt{\sigma'_{vo}/\sigma_{atm}}}\right) - 0.675\right]$$

The resulting initial relative density with depth computed using the Mayne (2007) correlation is shown in Figure 3.13, and ranges from approximately 40 to 50 percent. The improvement of this target zone will be shown in Section 3.3 as a function of pile spacing, drainage, and time.

The quantification of fines content, *FC*, is critical for the assessment of liquefaction susceptibility and performance of possible ground improvement measures. The *FC* from laboratory testing are helpful, but samples were tested at intervals ranging from approximately 0.75 m to 1.5 m and are therefore relative scarce. Owing to the usefulness of the CPT for stratigraphic profiling, Robertson and Wride (1998) proposed a global CPT-based *FC* correlation using the soil behavior type index, I_c, to make estimates of fines content in the absence of soil samples and their impact on liquefaction triggering. Since then, it has been shown that geologic unit-specific fines content correlations are significantly more reliable. Therefore, suitable CPT-based estimates of the *FC* at the test site were made using a fines content correlation developed specifically for the coastal beach sands of South Carolina using the measured fines from 152 split-spoon samples and corresponding I_c from nearby (within 0.45 m to 1.5 m) baseline CPTs over the corresponding depth interval. The functional form of the *FC* correlation proposed by Boulanger and Idriss (2014) was fitted to the measured data,

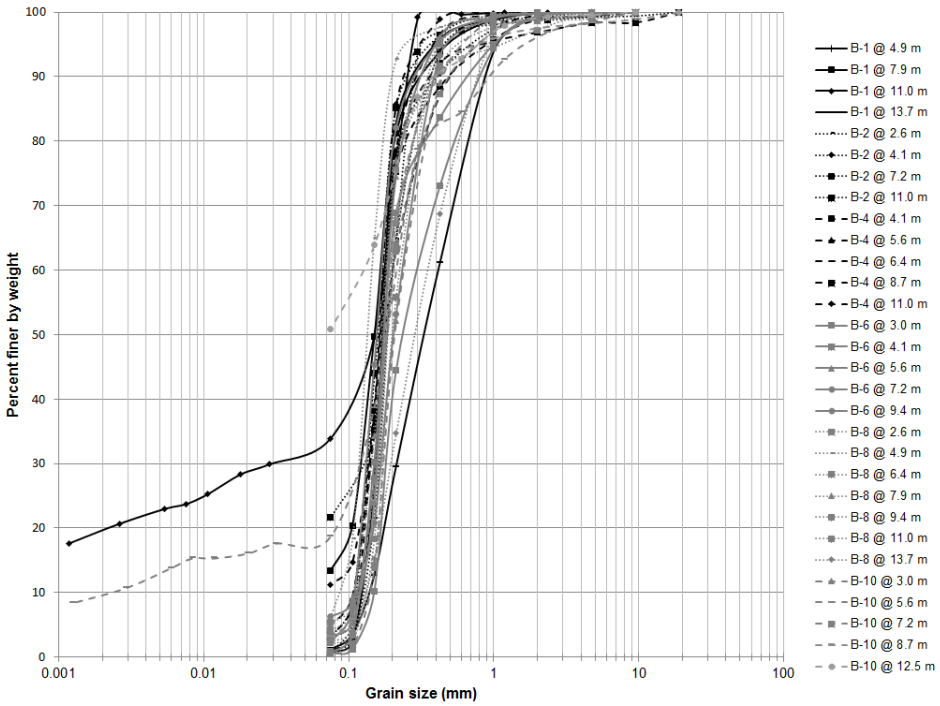

FIGURE 3.12 Grain size distributions of soils retrieved from the test site.

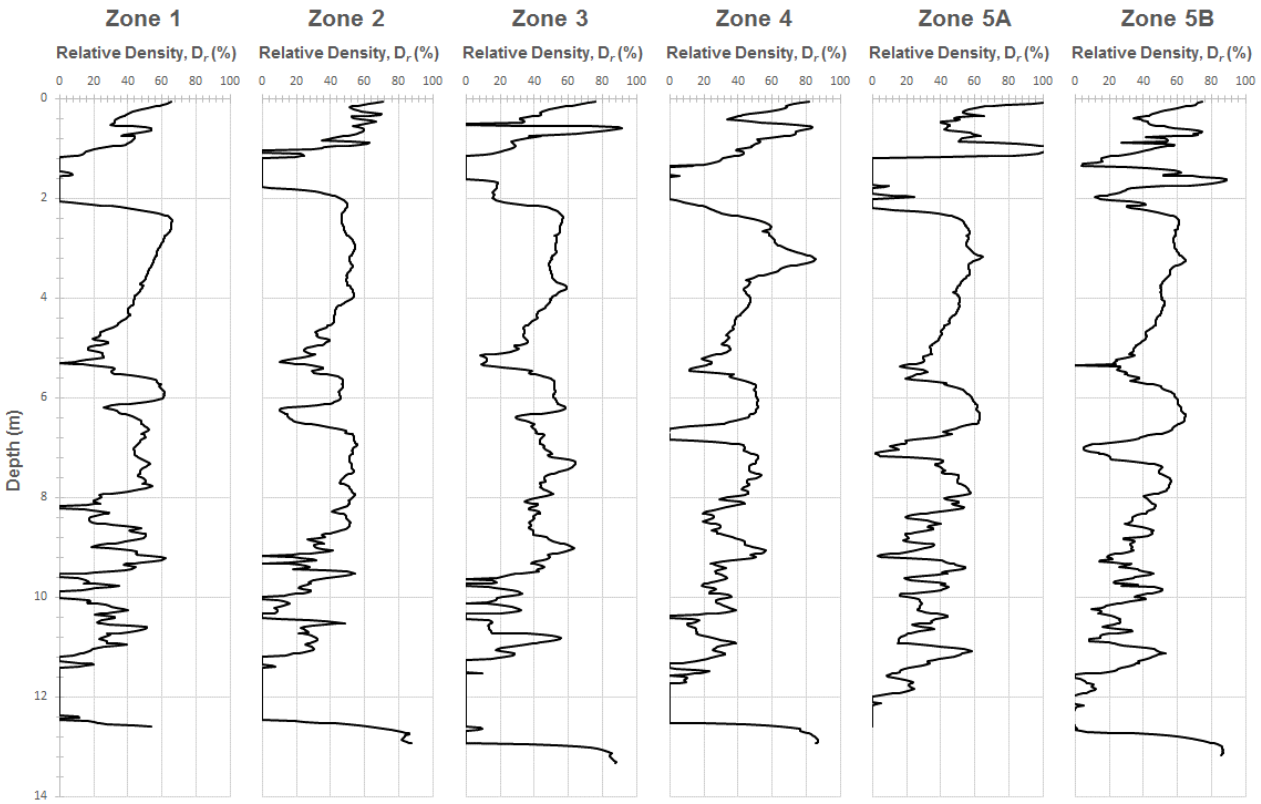

FIGURE 3.13 Initial (pre-installation) relative density based on CPT correlation.

plotted in Figure 3.14, resulting in the following site-specific *FC* correlation suitable for the beach sands of coastal South Carolina:

$$FC = 54 \cdot I_c - 101$$

The fines content profile estimated using the site-specific *FC* correlation is compared to the measured fines content from split-spoon samples from the borings in the center of each zone in Figure 3.15, and indicates satisfactory performance.

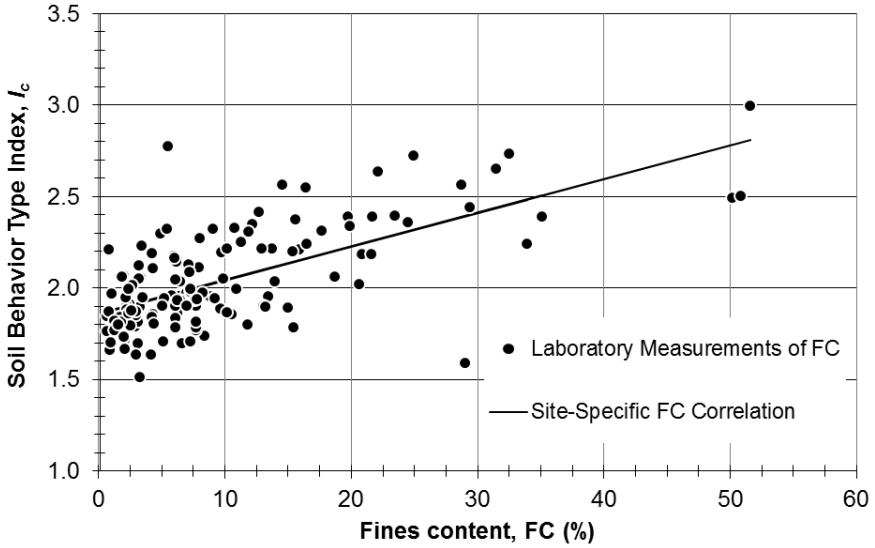

FIGURE 3.14. Comparison between measured *FC* and I_c and the site-specific correlation (n = 152).

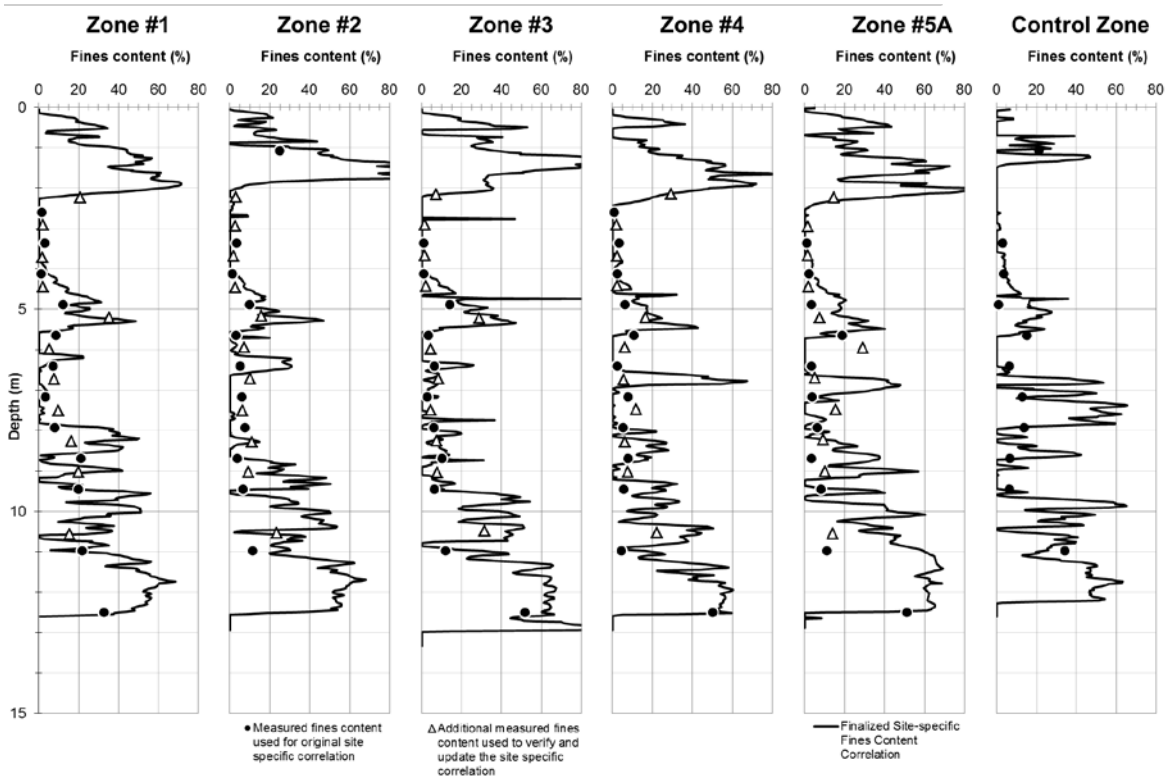

FIGURE 3.15. Comparison of measured *FC* and that estimated using the site-specific correlation.

3.2.4 Finalized Subsurface Model

The finalized subsurface cross section representative of the test area is presented in Figure 3.16. The soil stratigraphy consists of a 2- to 2.5-m-thick layer of clayey and silty sand fill, overlying a 9-m-thick layer of liquefiable clean to silty sand, overlying a 1-m-thick stratum of clay, and followed by a deposit of non-liquefiable dense sand. Between the depths of approximately 2.5 and 4 m below the ground surface the soil is relatively clean (i.e. fines content ranging from 1 to 10 percent); the soil below this depth to about 11.0 m becomes interbedded with silty sand and fines ranging from 0 to 40 percent. The region between approximately 2.5 and 11.0 m below grade consists of a loose to medium dense, saturated, sand susceptible to liquefaction. This is the stratum where ground improvement with conventional and drained timber piles was targeted and where blast-induced excess pore pressures have been triggered for comparison among the improved and unimproved zones. The liquefiable layer is bounded by an upper layer consisting of unsaturated silty to clayey sand fill with debris and a soft clay layer extending to the dense to very dense sand bearing layer, the latter of which begins at depths varying between 12.5 to 13 m.

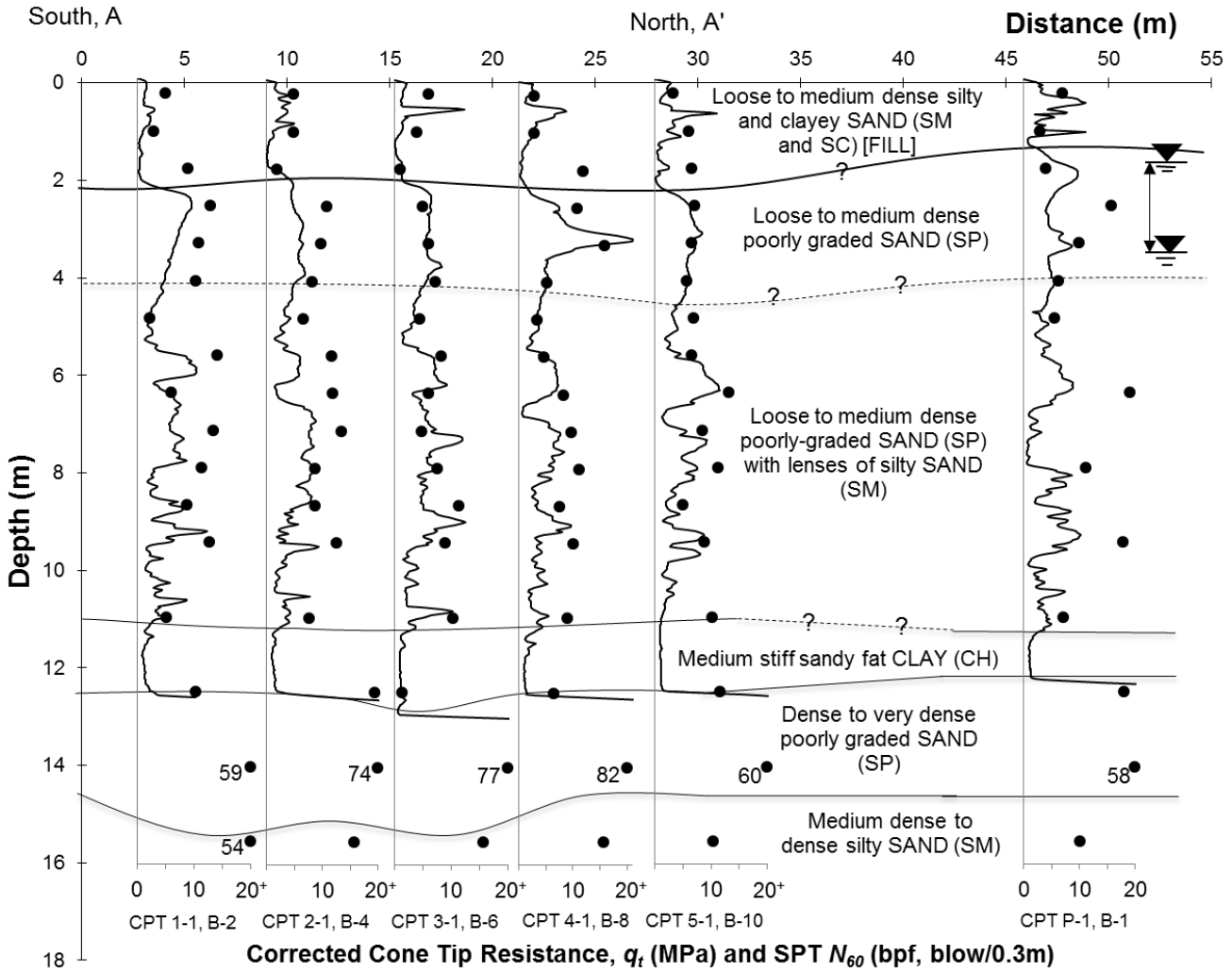

FIGURE 3.16 Finalized soil profile representing site stratigraphy in the test and control zones. The numbers adjacent to select SPT values indicated blow count when greater than 20.

3.3 Effect of Pile Spacing, Drainage, and Time on Densification

Ground improvement methods are typically implemented to achieve one, or sometimes two improvement mechanisms, such as drainage and densification. The use of multiple ground improvement methods on the same site can be costly and inefficient. Currently, no technology has been proven to provide reliable densification, reinforcement, and drainage in one application. This research proposes the use of a drained timber pile that may be a viable alternative. This alternative approach is intended to provide (1) densification of the surrounding soil, particularly liquefying soils with low hydraulic conductivity, such as fine sands and silty sands by draining driving-induced excess pore pressures; (2) the *potential* to reduce excess pore water pressures during earthquake shaking; and (3) the addition of shear and flexural reinforcement to the soil. This section documents the investigation of the ground improvement potential (i.e., densification) with respect to pile spacing, drainage, and time elapsed since installation. A controlled blast program was conducted at the control zone and the timber pile test area to evaluate the effectiveness of this ground improvement alternative to reduce blast-induced excess pore-water pressures and is described in Section 3.4.

3.3.1 Test Pile Program

As a result of in situ and laboratory testing, the liquefiable zone was identified between the depths of approximately 2.5 and 11.5 m below grade, and a dense bearing layer was identified at approximately 12.5 m to 13 m below grade. Based on these in situ tests, the timber piles were planned to be driven through the liquefiable soil layer and into the dense sand layer to approximately 0.5 m of penetration into the bearing layer with the tip of the pile at approximately 13 m to 13.5 m below grade. Owing to the use of standard pile lengths in South Carolina, the pile driving contractor elected to use 12.3 m long piles, rather than the next longest option of 13.8 m long piles, and to drive the piles approximately 0.7 to 1 m below grade to reach the target depth, following local convention. In order to calculate the change in relative density as a function of volume replacement, as discussed subsequently, the dimensions of the timber piles were required. The pile head and toe diameters of 33 randomly selected timber piles were measured to determine the average pile size. The average pile head and toe diameters were equal to 0.31 and 0.21 m, respectively, with as standard deviation of 18 and 14 mm, respectively. The typical pile taper was equal to 8 mm/m (0.1 in./foot).

The initial and as-built layout of the drained and conventional piling is shown in Figure 3.17. The five test zones proceed from Zone 1 along the southern portion of the site to Zone 5 in the north. The control zone lies approximately 15 m northeast of Zone 5 (compare to Figure 3.9), and is an unimproved area used as a baseline to compare the blast-induced pore pressures against the improved zones. Zones 1 and 3 and 2 and 4 correspond to piles spaced at 5 and 3 pile

head diameters (*D*), respectively. The drained piles are located in Zones 1 and 2 (i.e., Zone 5DPVD and 3DPVD, respectively). As shown in Figure 3.17, the planned 7x7 pile group at 2D spacing was altered in the field during installation as the progress of driving the piles was significantly impacted by the magnitude of densification being realized. Piles in this zone consistently wandered and buckled in response to the driving stresses imposed and resistance encountered. Thus, the zonal spacing was changed to 4D so as to improve the resolution of the spacing effects.

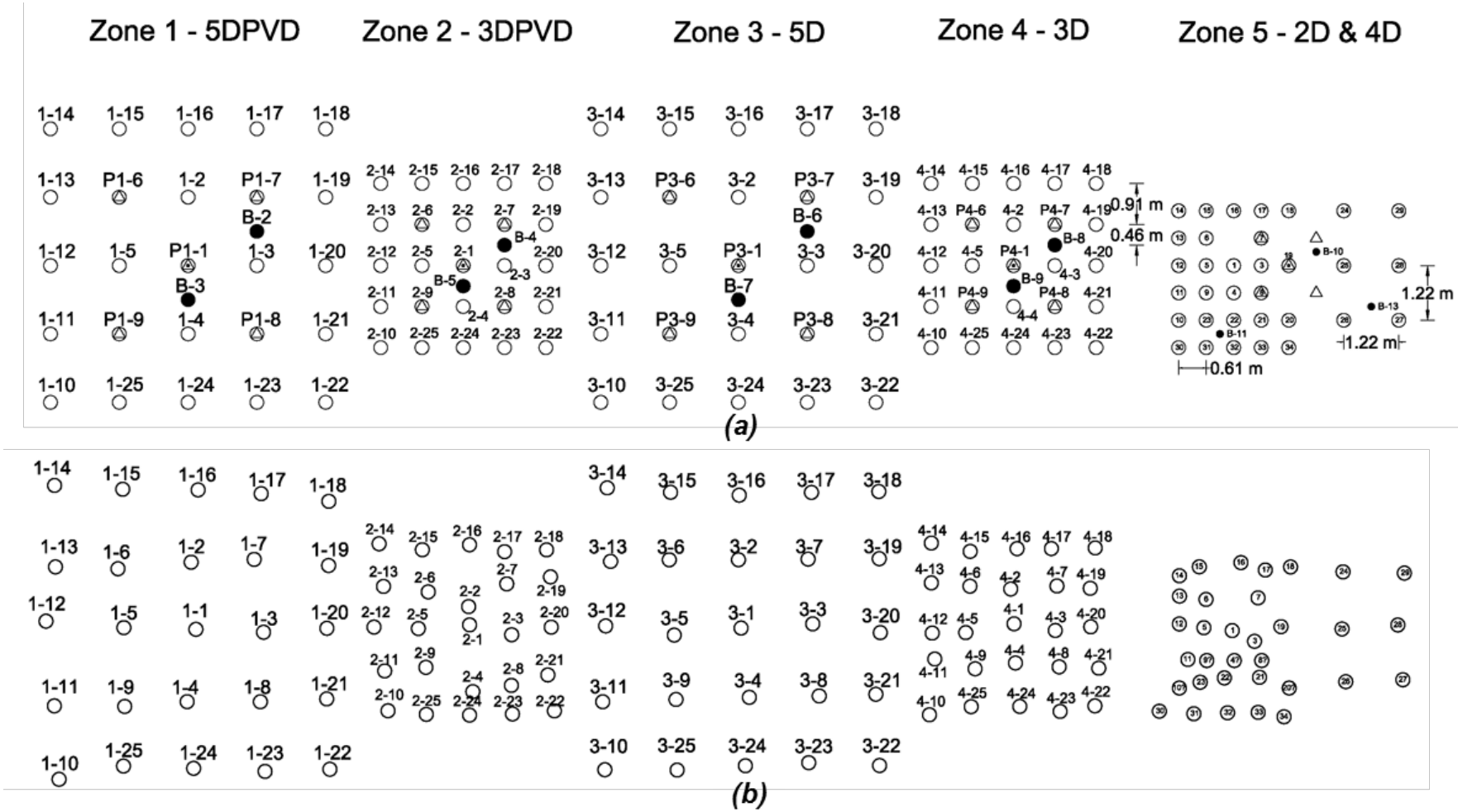

FIGURE 3.17 Layout of timber pile test program indicating (a) planned location of drained (PVD) and conventional piles (compare to Figure 3.10), and (b) actual as-built location of drained and conventional piles (survey measurements at pile head). *Note*: Zone 5 was altered from a 7 x 7 pile group at 2D spacing to 2D and 4D spacing based on observed driving response and damage to piles at 2D spacing. Densification at 2D was so great as to prevent reliable installation of the piling.

To evaluate the effect of spacing, elapsed time, and drainage on the amount of soil densification, an in situ test program was planned and executed for comparison against the baseline tests conducted prior to ground improvement. Figures 3.10 and 3.17(a) show the explorations conducted to establish the baseline condition. Four "cells" (e.g., B2, B3, C2, and C3) in the middle of each pile group were selected to represent a theoretically uniform level of ground improvement within the pile group (Figure 3.10). Figure 3.18 presents the test plans formulated to evaluate the effect of time on densification. Each of these cells, B2, B3, C2, and C3, should represent equal trial areas allowing the observation of the time effect, barring the effect of spatial variability of the soil and as-built pile position. Each cell was tested three times, indicated as points A, B, and C in Figure 3.18. Point A is located in the mid-point of each cell, and is anticipated to reveal the minimum amount of densification; as such, it was always conducted first, so as to eliminate the potential for disturbance following testing at the other locations. Points B and C were closer to the piling and were intended to help understand the radial distribution of densification. The CPT test plan layout was slightly different for Zone 5 (Figure 3.19) due to the change in pile layout, but the same methodology was followed (i.e., pushing A, B, then C where applicable). Table 3.2 indicates the average number of days that the CPT soundings were performed following pile installation and the cell locations corresponding to Figures 3.18 and 3.19. An expanded view of an individual cell (e.g., B2 and E1) for the typical CPT sounding layouts shown in Figures 3.18 and 3.19 is provided in Figure 3.20 (Zones 1 through 4 and 5A) and Figure 3.21 (Zone 5B), respectively. The CPT sounding locations relative to the planned timber pile locations and corresponding to these figures are shown in Table 3.3. CPT soundings A, A-1, A-2, and A-3 were always pushed first in each cell to stay consistent, testing the center of the improved area prior to creating any voids or further densification as a result of the other CPTs pushed in close proximity.

Table 3.2. Test cell location of CPTs following timber pile installation

Time Following Installation	Cell Locations (Zones 1 through 4)	Cell Locations (Zones 5A and 5B)
10 days	B2	B3 and E1
49 days	B3	B4 and E2
115 days	C2	C3 and F1
255 days	C3	C4 and F2

Table 3.3. Spacing of CPT soundings relative to timber piles following installation

Zone No. (Reference Figure No.)	(Pile Spacing) (meters) *D*	E (cm)	F (cm)	G (cm)	H (cm)
1–4 (3.18)	0.91 (3*D*)	23	31	46	50
1–4 (3.18)	1.52 (5*D*)	31	61	76	93
5A (3.19)	0.61 (2*D*)	N/A	15	31	28
5B (3.19)	1.22 (4*D*)	32	46	61	71

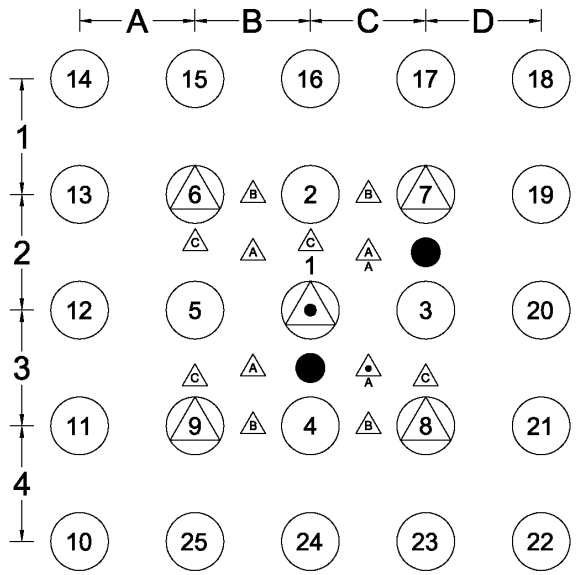

FIGURE 3.18 Typical post-installation in situ test plan for Zones 1 through 4.

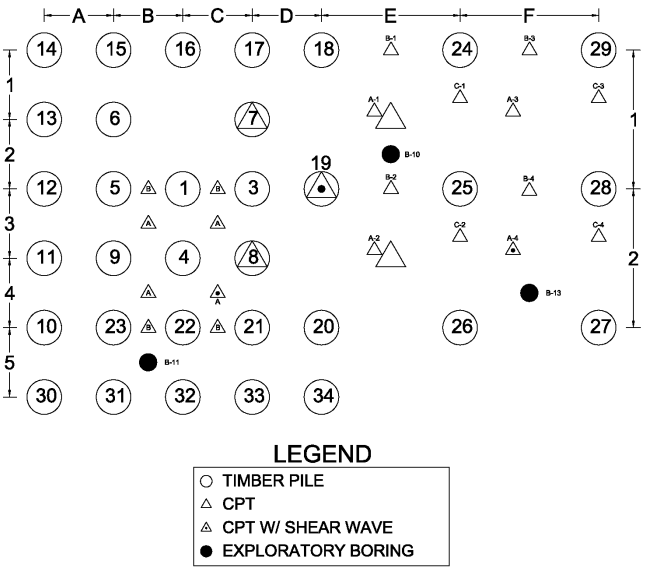

FIGURE 3.19 Typical post-installation in situ test plan for Zones 5A (2D) and 5B (4D).

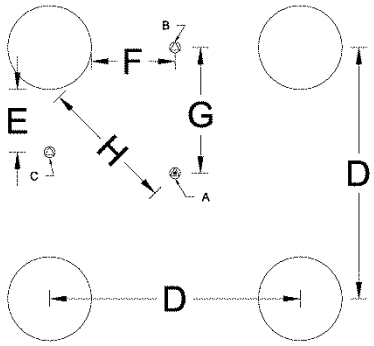

FIGURE 3.20 Cell spacing detail and CPT test plan for Zones 1 through 4 and 5A.

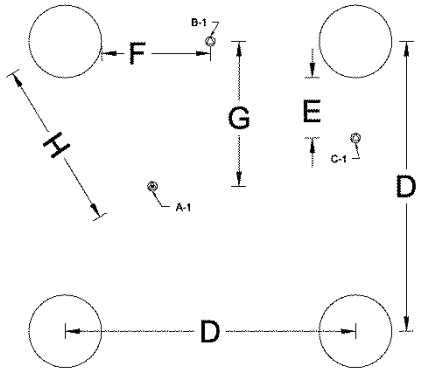

FIGURE 3.21 Cell spacing detail and CPT test plan for Zone 5B.

3.3.2 Evaluation of Pile Spacing on Densification

The effect of pile spacing on densification is first assessed using sounding A for each cell. Then, soundings B and C are compared to sounding A, below, to assess the effect of radial distribution of densification from the pile. The first round of CPTs were performed approximately 10 days following installation, and the relative density, D_r, improved to approximately 70 and 80 percent in Zones 3 and 4 (5*D* and 3*D* spacing), respectively, in the upper 2.5 to 5 m, and to approximately 60 to 75 percent in the range of depths of 5 to 9 m for both pile spacings (Figure 3.22). Initially, the relative density, D_r, in these zones ranged from 40 to 50 percent (Figure 3.13), resulting in absolute increases in D_r of 20 to 40 percent. The 49-day CPT soundings in Zone 5A and 5B at spacings of 2*D* and 4*D*, respectively, refused between depths of 4 and 6 m below grade. Owing to the observed refusal of the in situ test equipment, an alternative approach for the estimation of relative density was developed assuming that the volume of soil voids would be reduced by an amount

equal to the volume of the pile and equally distributed across the respective tributary area. In other words, the volume of a quarter pile, half pile, and whole piles was removed from the volume of soil voids in the tributary area of corner, side, and interior piles respectively, and the new relative density computed. This approach required the estimation of minimum and maximum void ratio, which was determined as described by Gianella (2015). The average timber pile taper was taken into account in the volume replacement-based relative density computations. Additionally, the relative density estimated with the volume replacement approach varied with each "cell" (e.g., B2 or C3), since each pile location was pre-drilled and the pile toes were installed to different depths.

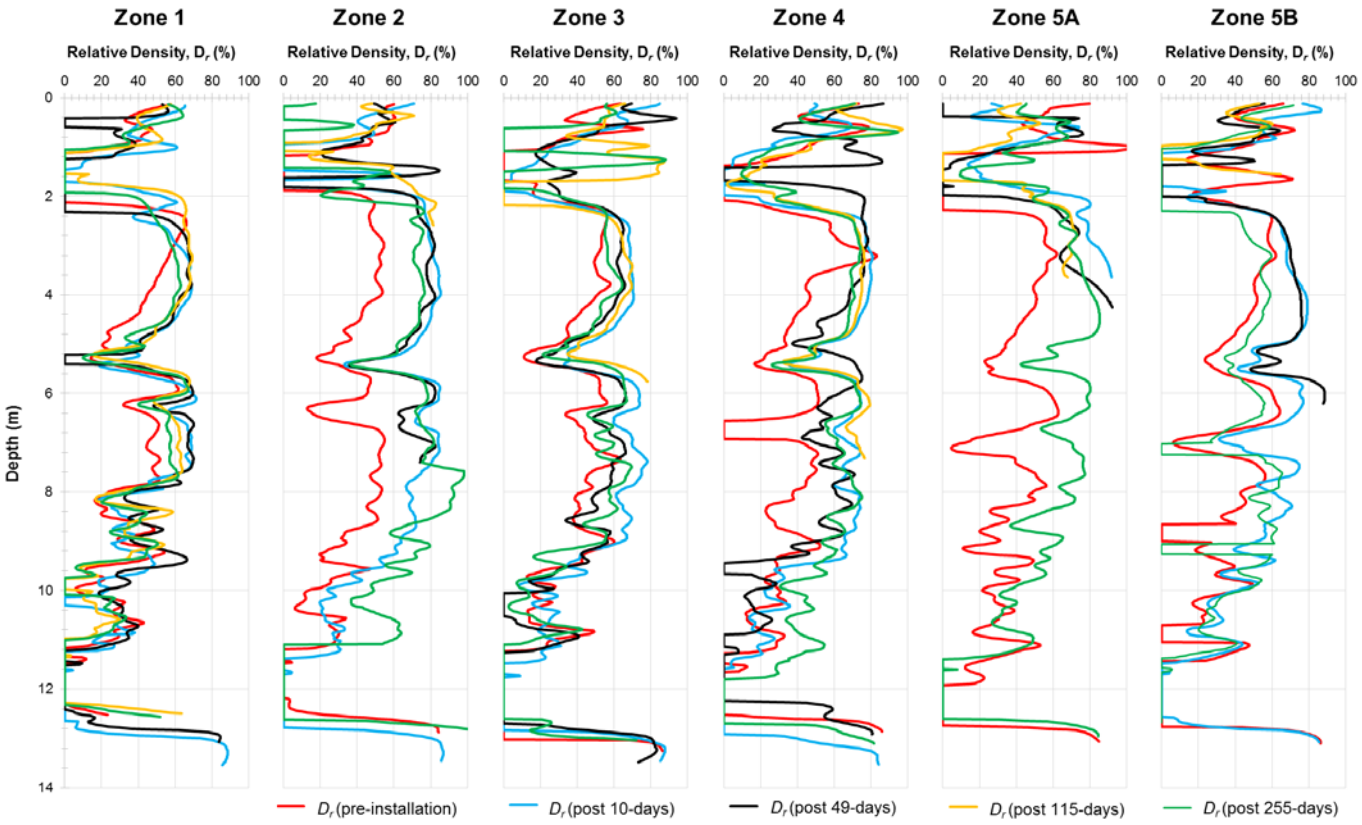

FIGURE 3.22. Relative density as correlated from cone tip resistance for the baseline and post-improvement cases. The D_r values have been smoothed using a 9-cell geometric mean over a 0.16 m interval (i.e., smoothing window).

Using the alternative volume replacement approach, the relative density in Zones 5A and 5B was expected (i.e., predicted) to reach between 80 to 100 percent for the 49-day soundings, as shown in Figure 3.23. This figure also includes the measured pre-improvement baseline and post-improvement relative density at 49 days for direct comparison to the volume replacement approach. The expected and observed improvement decreases with depth as a function of the pile taper and increasing fines content. At depths of approximately 11.5 m to 12.5 m, corresponding to the clay layer in Figure 3.16, the improvement is minor. The increase in relative density estimated using volume replacement approach was consistent with CPT refusal. Comparison of the CPT-based relative density to the volume replacement method shows

that the 115-day CPT soundings could have been expected to encounter refusal in consideration of the cell-specific pre-drill depths and pile lengths; refusal was in fact frequent at 115 days. The only 115-day sounding that was able to be pushed to the desired depth (i.e., 12.5 m) was in Zone 1. Figure 3.22 shows the refusal depths in Zones 2 through 5. The 115-day CPT soundings in Zones 3 and 4 were stopped between depths of 6 to 8 m below grade, and Zones 2, 5A, and 5B were only pushed to depths of approximately 2 and 4 m below grade. Based on Figure 3.24, similar refusal depths were expected for the 115-day soundings. This figure shows that the relative density for the 115-day soundings in cells C2, C2, C3, and F1 for Zones 2, 4, 5A, and 5B, respectively, were also expected to reach between 80 to 100 percent based volume replacement of the pile.

Either the soil in each zone had been densified to such a high degree or debris was encountered such that pushing the cones the entire depth of the soil profile was extremely difficult. The project team indicated the importance of obtaining full depth soundings at the 8-month testing interval to compare cone tip resistance and relative density to the initial conditions. It was recommended that a different CPT rig to provide greater reaction force or offsetting the cone a few inches to prevent premature refusal. As shown in Figures 3.22 and 3.26, the 255-day soundings reached the desired penetration depth of approximately 12.5 m below grade, but the CPT-based D_r in each zone was not consistently greater than or equal to the previous soundings. Soundings A-4 and B-4 in Zone 5B were unable to be pushed to full depth after many attempts.

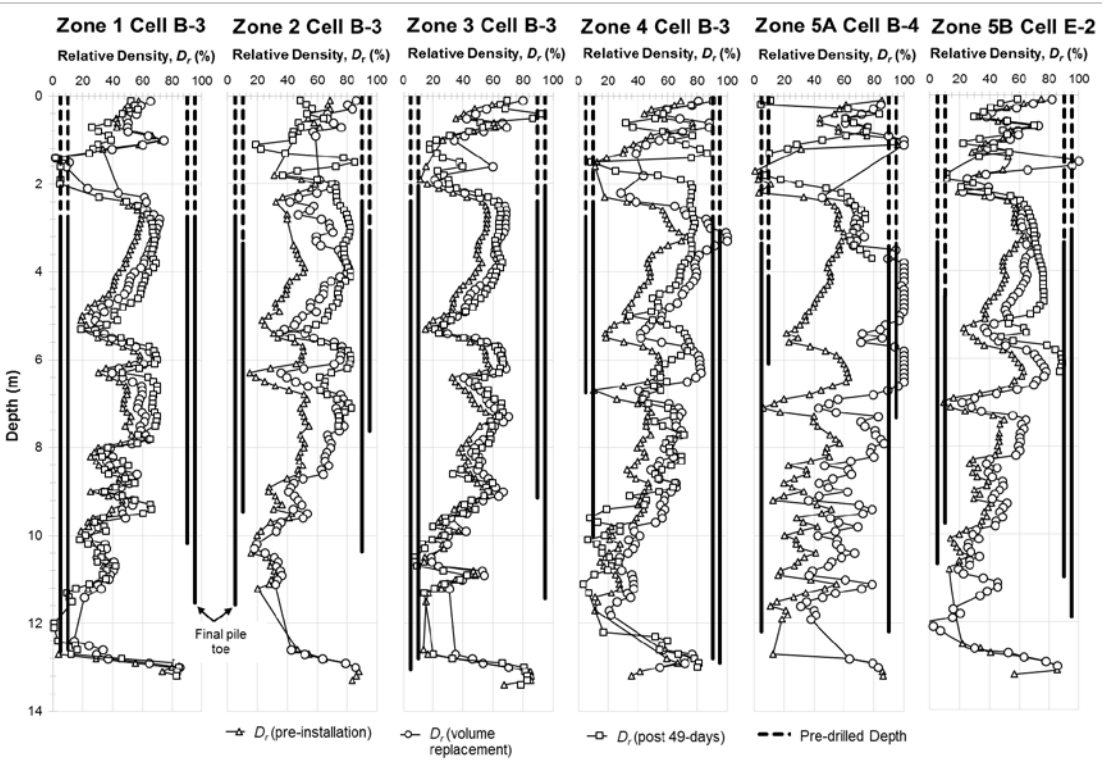

FIGURE 3.23 Pre- and post-installation relative density derived from cone tip resistance and the volume replacement approach for measurements 49 days following installation.

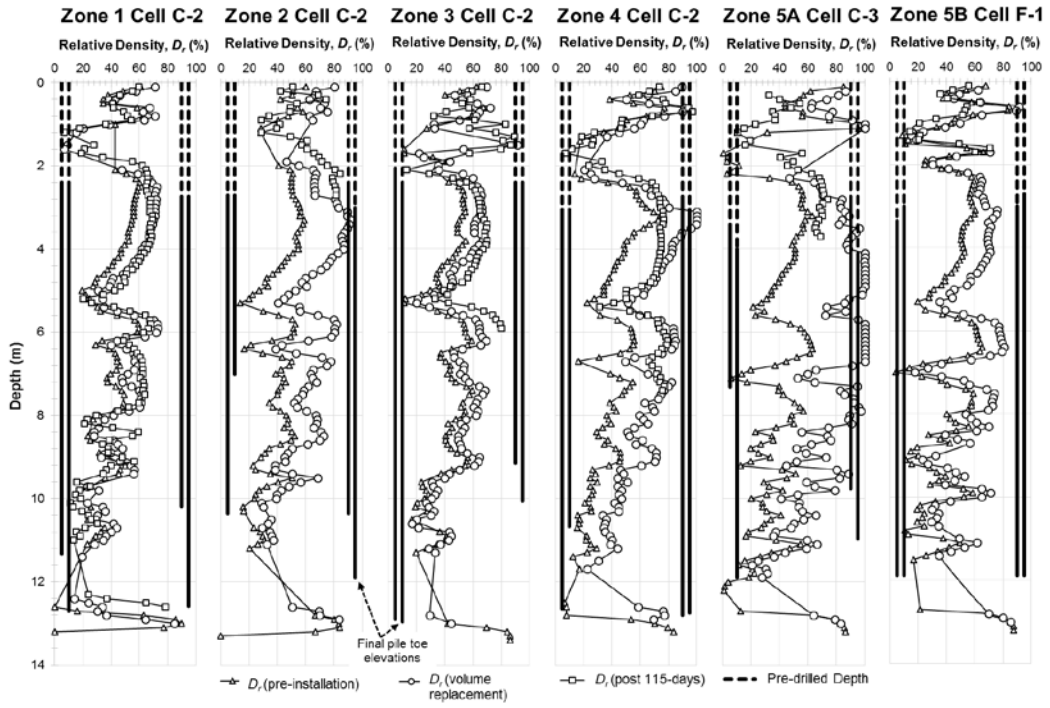

FIGURE 3.24 Pre- and post-installation relative density derived from cone tip resistance and the volume replacement approach for measurements 115 days following installation.

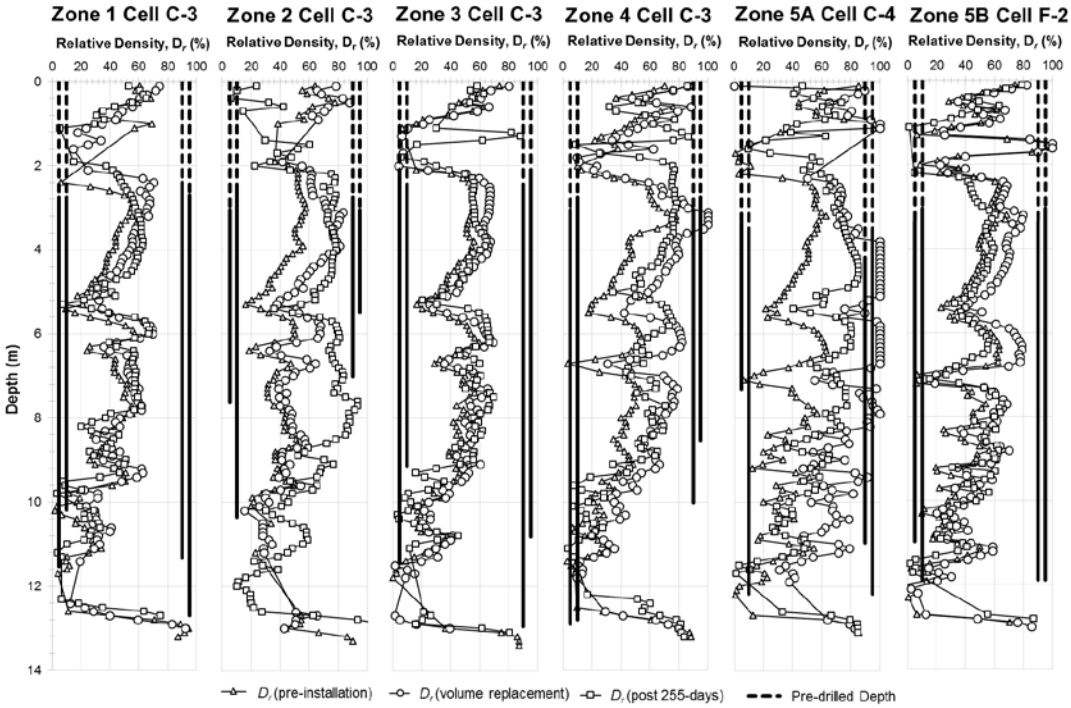

FIGURE 3.25 Pre- and post-installation relative density derived from cone tip resistance and the volume replacement approach for measurements 255 days following installation.

Figure 3.26 compares the effect of radial distribution of densification with distance from the pile. The locations of soundings A, B, and C for each zone in the figure correspond to Figure 3.20 with individual distances to the timber piles

as shown in Table 3.3. In general, q_t increases with decreasing distance towards the pile (i.e., sounding C > B > A). To quantify the improvement with distance from a timber pile, the post-improvement q_t values corresponding to soundings from all zones with nearly identical spacings were averaged and plotted versus depth, as presented in Figure 3.27. For example, soundings 1C, 3C, 2B, and 4B are all approximately 31 cm from the closest pile in their respective cells. As expected, q_t increases as the sounding location decreases from 93 to 16 cm away from the pile, although the data measured at an offset of 50 cm appears more dense that that at 31 cm. The average corrected tip resistance for the soundings 16 cm from the pile was approximately 10 MPa larger than the soundings 93 cm from the pile between the depths of 4 and 11 m. This trend is less evident between 0 and 4 m, where pre-drilling of pile locations was conducted, and 11 and 13 m below grade.

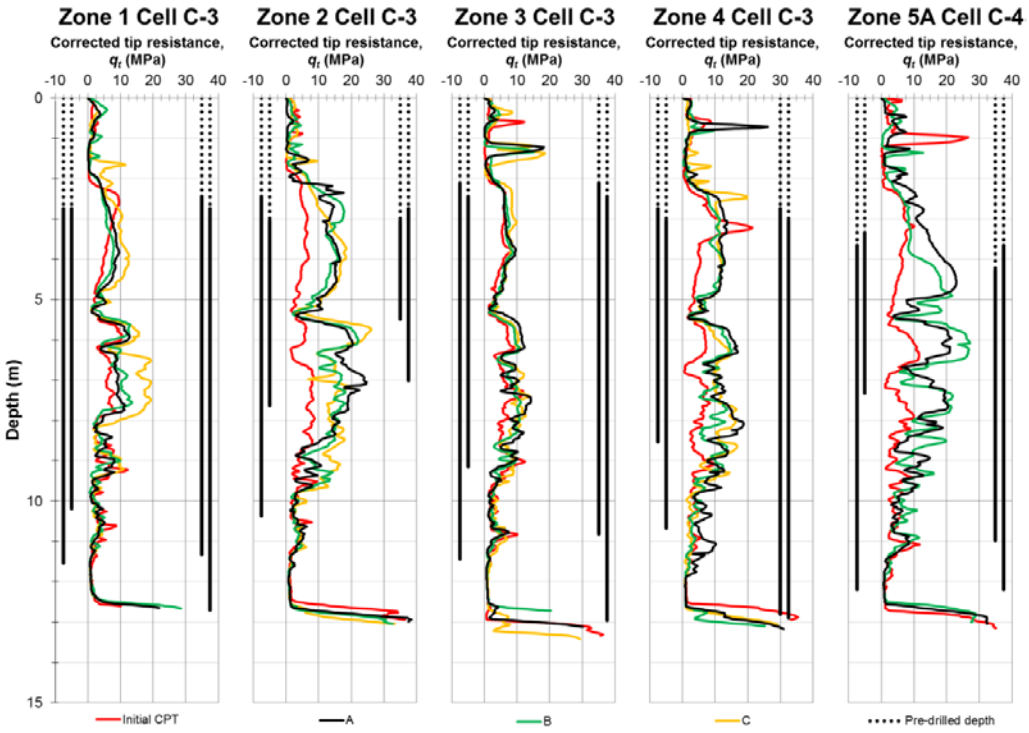

FIGURE 3.26 Baseline and 255-day post-improvement corrected tip resistance for Zones 1 through 5 displaying the effect of radial distribution per cell.

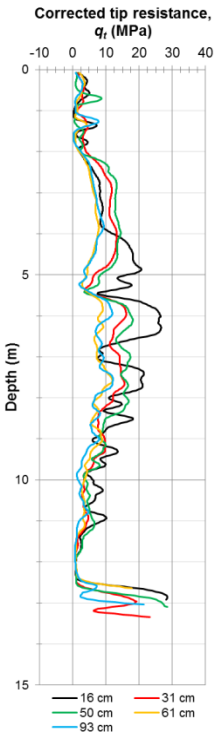

FIGURE 3.27. Effect of densification with distance from pile.

Post-installation SPTs were performed in each zone (i.e., B-3, B-5, B-7, B-9, B-11, and B-13 in Figure 3.17) at an average of 292 days following pile installation at the test site to provide additional quantification of the ground improvement. These SPTs were completed using a truck-mounted CME-55 rig equipped with a cathead hammer by Carolina Drilling, Inc. It should be noted that cathead hammers can be inconsistent and dependent on the operator (Kulhawy and Mayne 1990), and the operator was observed switching arms throughout the duration of testing. Energy testing was performed by S&ME, Inc., using strain gauges and accelerometers attached to the AWJ drill rods. Based on

four energy tests at depths of 4.6, 7.6, 10.7, and 13.7 m below grade, the average hammer efficiency was determined to be equal to 59 percent.

In order to compare the SPT penetration resistances directly to the pre-installation values, N_{60} blow counts were calculated using the observed energy transfer efficiency. The pre- and post-installation N_{60} blow counts for each zone are presented as a function of depth in Figure 3.28. In general, improvement was observed in all zones below the fill (i.e., between 3 and 11 m below grade) until the soft sandy clay layer was reached. In this depth range, the post-installation N_{60} blow counts for Zones 1, 2, 3, and 5B were approximately 3 to 14 blows per 0.3 m larger than the pre-installation values. Zone 4 showed improvements in N_{60} (i.e., ΔN_{60}) ranging from 5 to 18 blows per 0.3 m. Zone 2 showed similar improvements to the Zones at 4*D* and 5*D* spacing instead of the other zone at 3*D* spacing. This trend can be explained by referring to Figure 3.17(b) of the actual pile locations surveyed "as built." Note that Pile P2-1 was installed very close to P2-2 and P2-4 was installed very close to P2-24 creating a larger spacing (i.e., ~ 5*D* spacing) between Piles 2-1 and 2-4 where the SPT was performed instead of the intended 3*D* spacing. The largest improvement was exhibited by Zone 5A with the 2*D* spacing, with N_{60} increasing by approximately 9 to 22 blows per 0.3 meters. The two large post-improvement magnitudes of N_{60} observed in Zones 2 and 3 at a depth of 1.37 m were a result of wood debris as indicated by the presence of wood in the tip of the sampler.

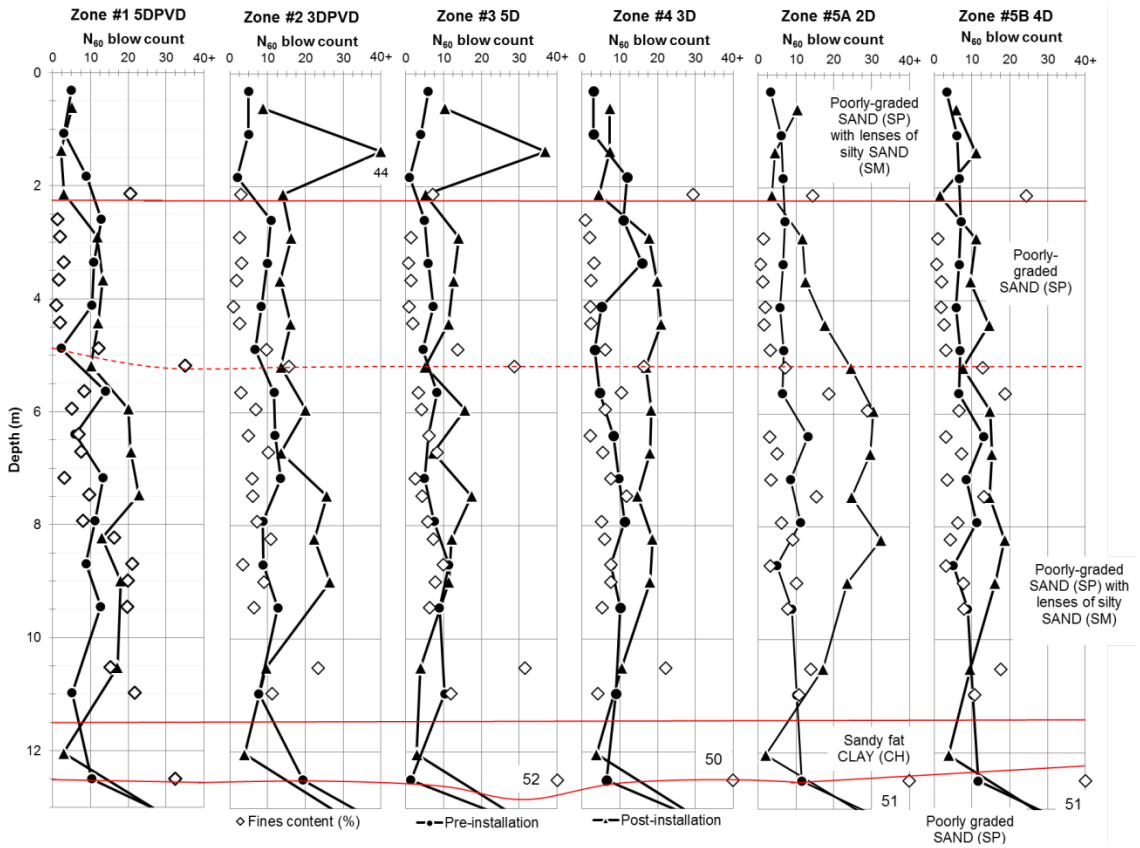

FIGURE 3.28 Comparison of pre- and post-installation SPT N_{60} values for depths of 0 to 13 m, only.

3.3.3 Effect of Drainage and Time

To evaluate the effect of time and drainage on the amount of soil densification, the drained piles in Zones 1 and 2 (5*D* and 3*D*, respectively) are compared to the conventional piles driven in Zones 3 and 4. Figures 3.23 through 3.25 showed that the liquefaction-susceptible soil in Zones 1 and 2 (i.e., drained piles) exhibited a larger improvement in D_r as compared to the D_r predicted using the volume replacement estimation approach. The improvement in D_r for the conventional piling was less than or equal to the improvement estimated using the volume replacement approach. The comparison is improved by considering the fines content of the soils. Figure 3.29 compares the smoothed D_r for each zone and for the 10-day, 49-day, 115-day, and 255-day soundings against the fines content. The effect of time-since-installation is expected to have little effect on the clean sands because densification occurs nearly instantaneously, but is expected to have a larger impact on the densification of the silty zones. The fines content increases to approximately 50 percent and 30 percent at depths of 5.25 m and 6.5 m below the ground surface, respectively. At these elevations, the 49-day D_r in Zone 2 has approximately a 5 to 10 percent larger improvement compared to the improvement observed in Zone 4 using conventional piles. The improvement was generally the same when comparing Zones 1 and 3 at 5*D* spacing in these silty regions. An expanded view of the improvement in q_t with time in these silty and clayey lenses is shown in Figure 3.30. In this figure, a consistent increase in penetration resistance with time is exhibited in the two upper silty regions of Zone 2. It was difficult to ascertain the improvement between the drained and conventional piles owing to the site variability per cell resulting in inconsistent trends with time, and deviations in position from planned pile locations.

Figures 3.31 through 3.34 compares the change in q_t for each zone with time, corresponding to 10 days, 49 days, 115 days, and 255 days following installation, respectively. Figure 3.31 shows the raw q_t values overlain by q_t averaged using the geometric mean taken over a 0.16 m interval. This allows for the pre- and post-improvement q_t with time to be compared directly accounting for minor spatial variability between the soundings. Figure 3.31 indicates that the smoothed q_t values are similar to the un-averaged q_t values; therefore only the smoothed q_t values are plotted in Figures 3.32 through 3.34. To quantify the average improvement of each zone based on penetration resistance, the difference between the pre- and post-installation q_t values was calculated for the liquefiable soil layer corresponding to the depths of 3.3 m to 11 m below grade. Tables 3.4 and 3.5 present the average of the q_t for pre- and post-installation conditions in each zone for the 10-day and 255-day soundings, respectively; these were selected for comparisons since the CPTs at these time intervals reached the desired penetration depths (except for the 10-day sounding in Zone 5A). The percent increase in q_t ranged from approximately 26 to 202 percent with the largest improvement in Zone 2 corresponding to the drained piles at 3*D* spacing. These tables show that the drained piles in Zone 2 exhibited larger increases in q_t than the conventional piles in Zone 4, but the performance in Zone 1 was similar to Zone 3 after approximately 8 months.

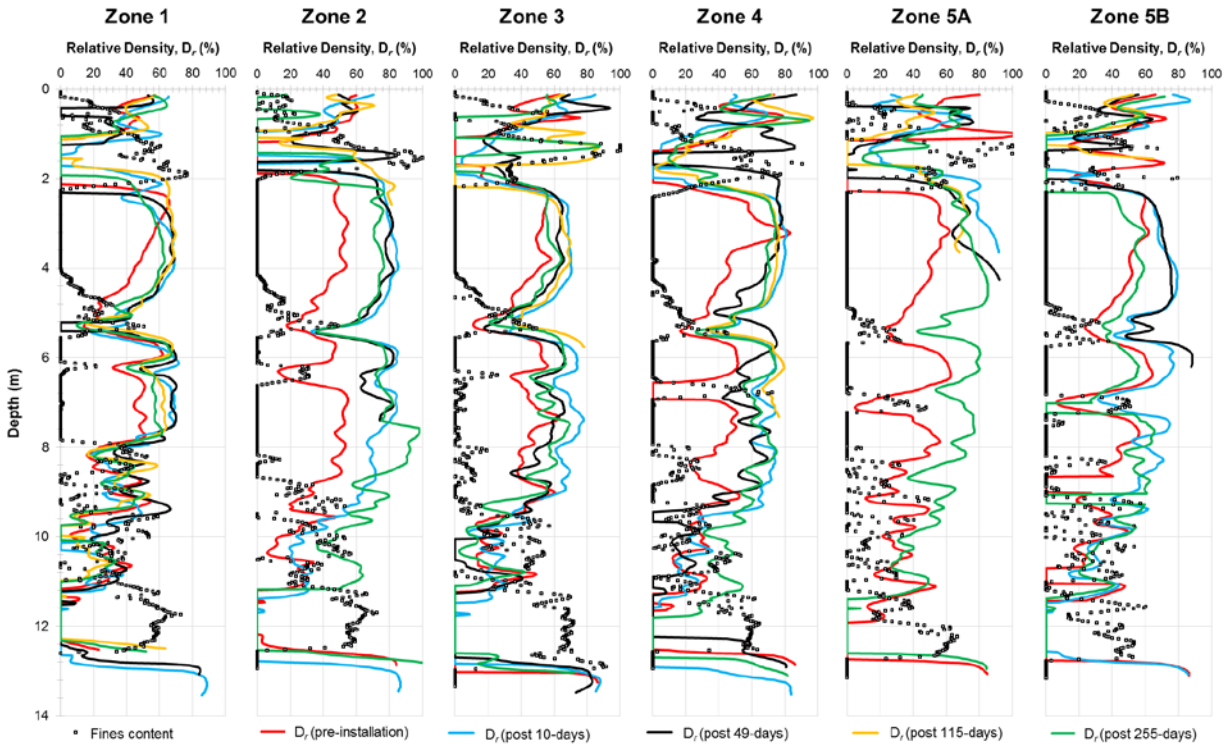

FIGURE 3.29 Baseline and time-elapsed post-improvement relative density for averaged (9-cell mean) conditions and fines content as correlated from cone tip resistance.

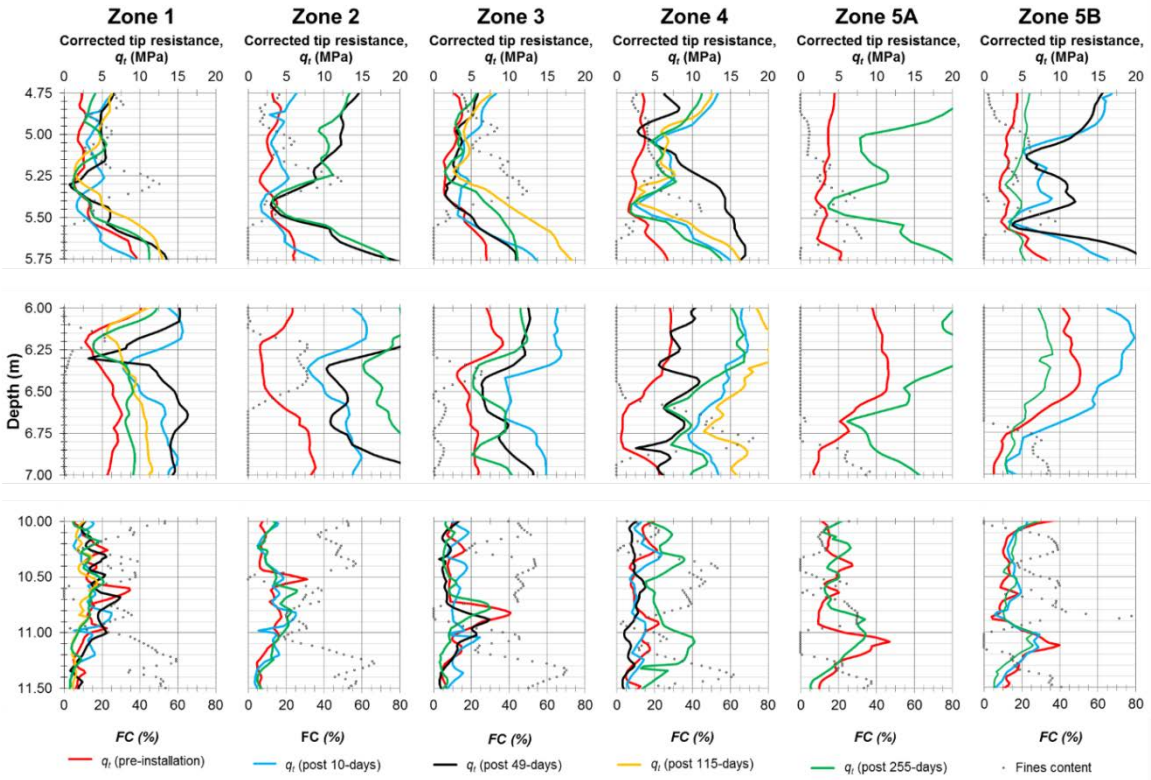

FIGURE 3.30 Baseline and time-elapsed post-improvement corrected tip resistance of Zones 1 through 5 evaluating regions containing high fines contents.

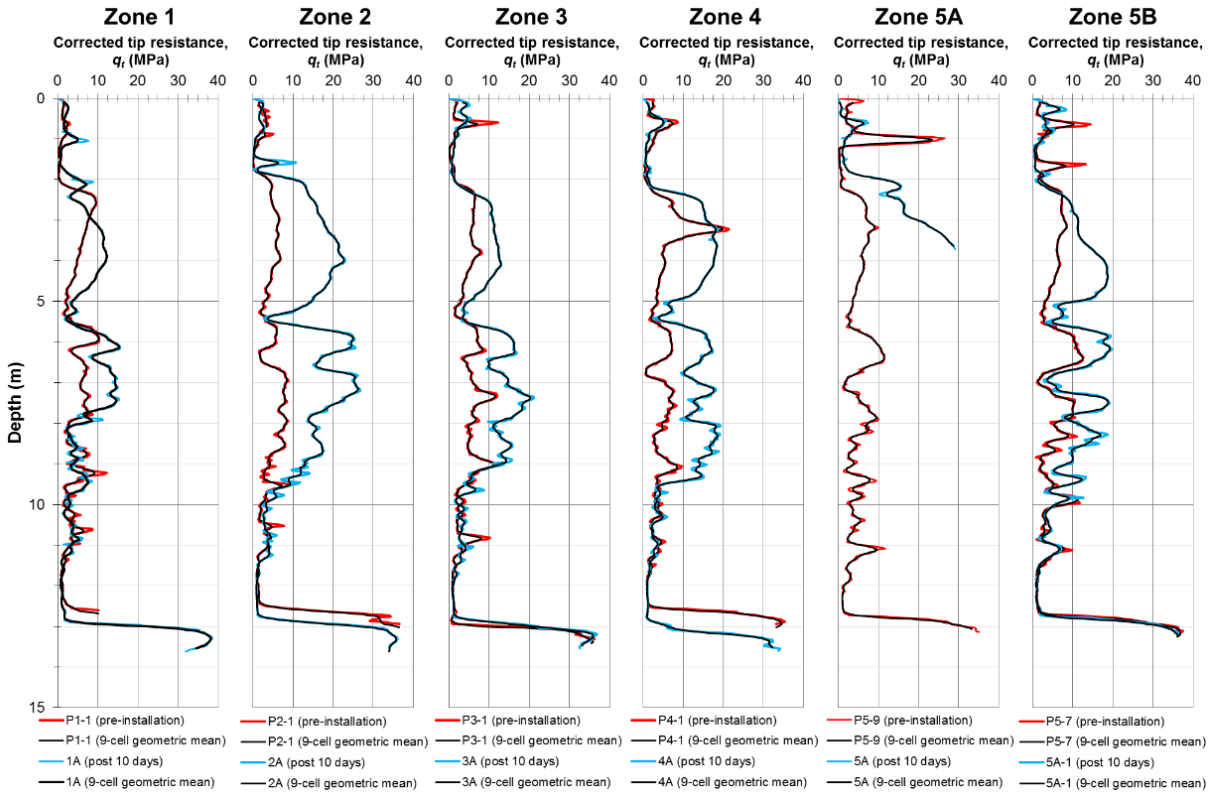

FIGURE 3.31 Baseline and 10-day post-improvement corrected tip resistance for averaged (9-cell mean) and non-averaged conditions of Zones 1 through 5.

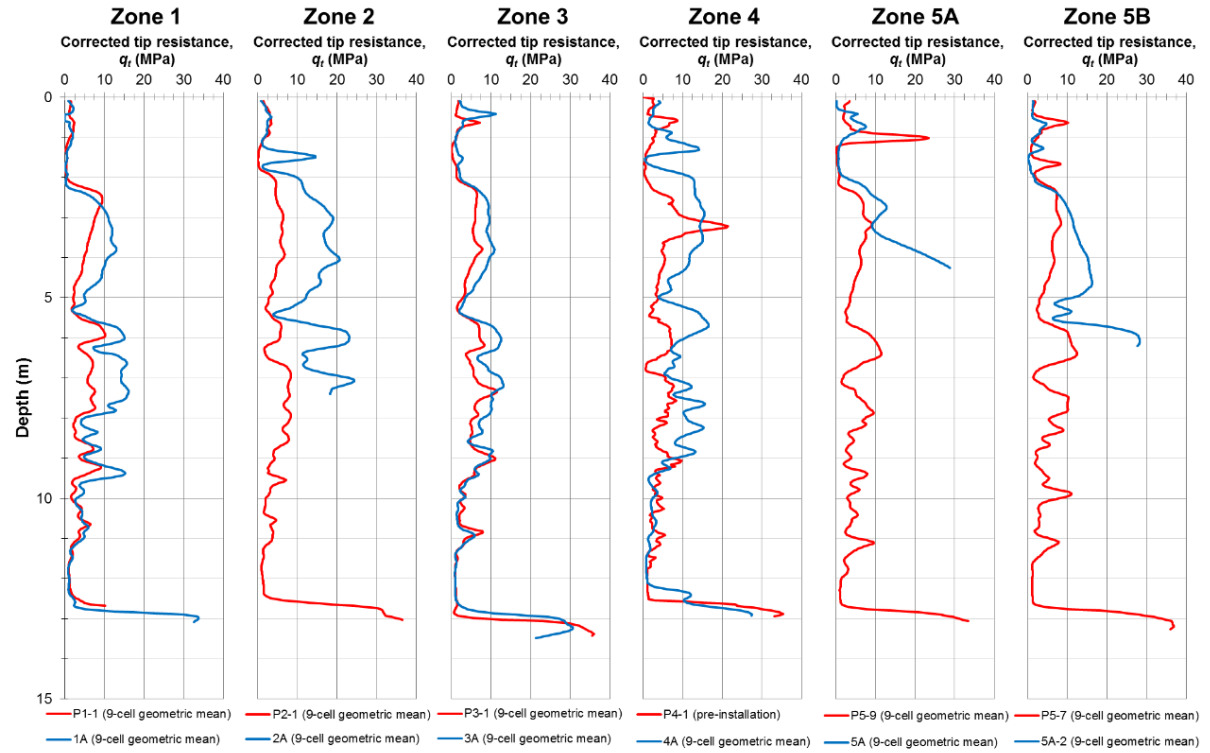

FIGURE 3.32 Baseline and 49-day post-improvement corrected tip resistance for averaged (9-cell mean) and non-averaged conditions of Zones 1 through 5.

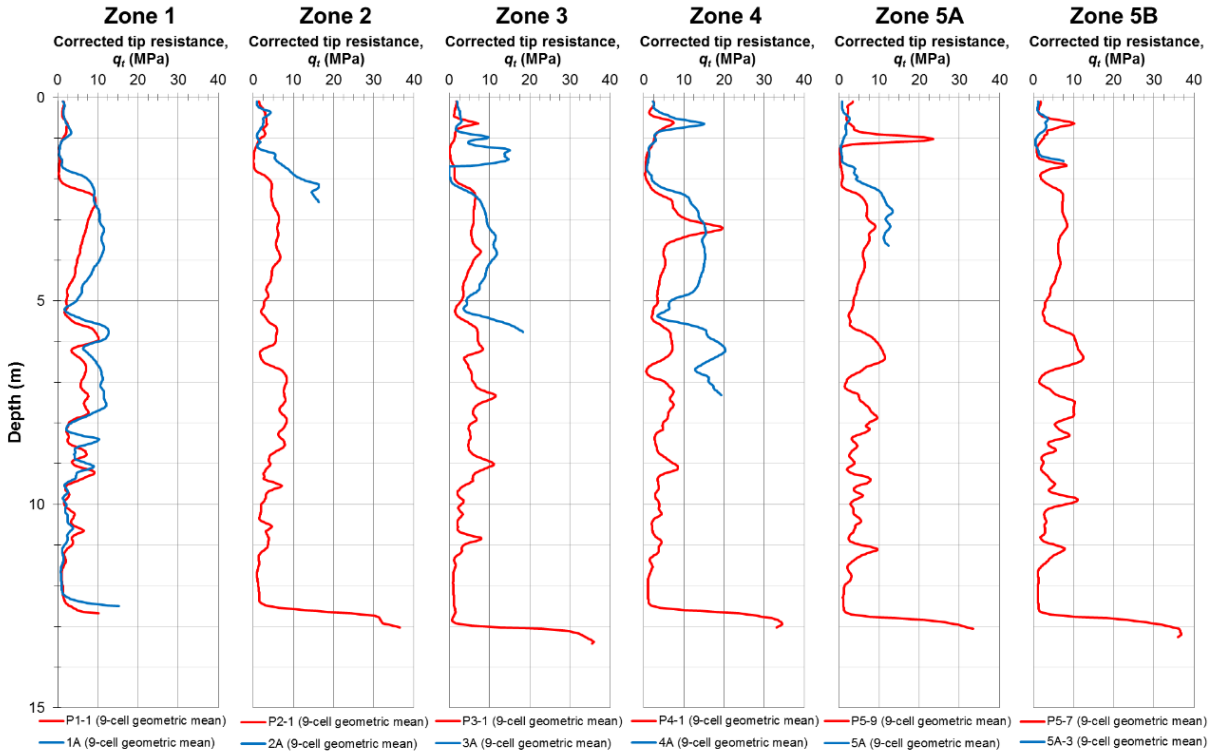

FIGURE 3.33 Baseline and 115-day post-improvement corrected tip resistance for averaged (9-cell mean) and non-averaged conditions of Zones 1 through 5.

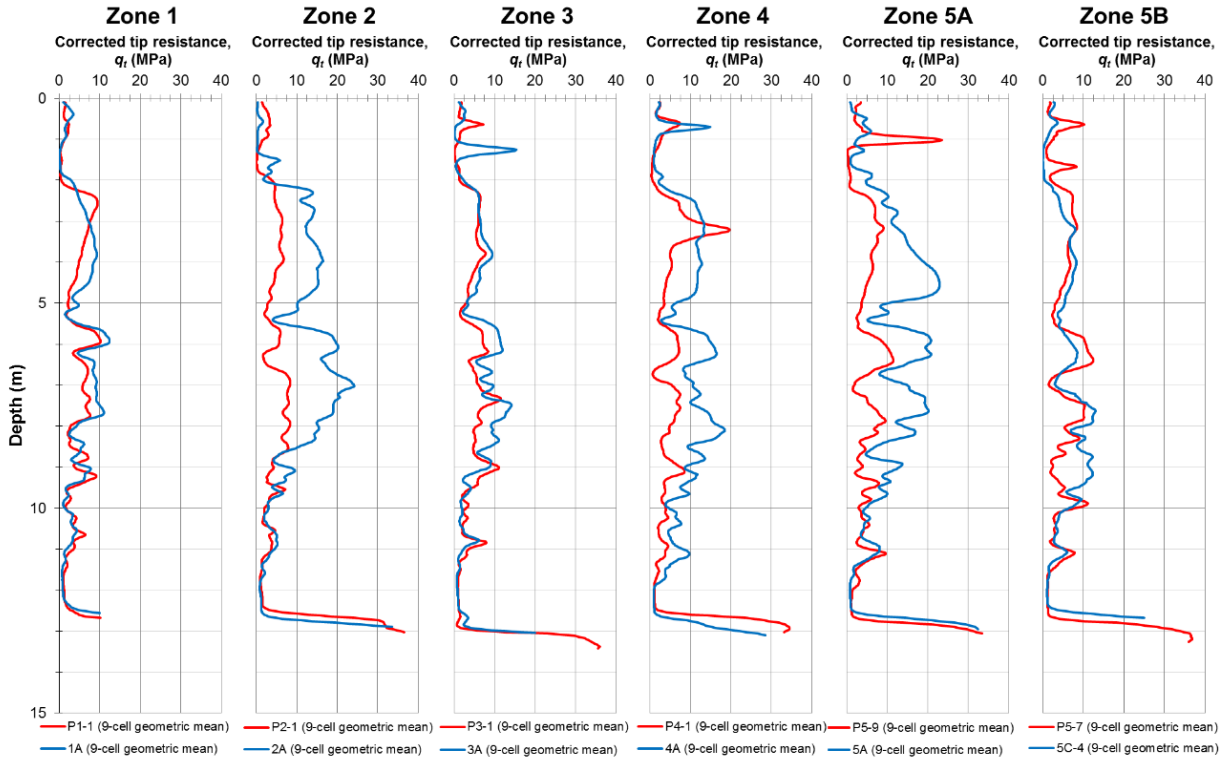

FIGURE 3.34 Baseline and 255-day post-improvement corrected tip resistance for averaged (9-cell mean) and non-averaged conditions of Zones 1 through 5.

Table 3.4. Average improvement in q_t using a geometric mean approach for the liquefiable soil layer in each zone for depths of 3.3 m to 11 m (10 days following installation)

Zone No.	Average Corrected Tip Resistance Pre-treatment (MPa)	Average Corrected Tip Resistance Post-treatment (MPa)	Average Δq_t (%)
1	4.9	7.6	57
2	5.0	15.0	202
3	5.3	10.2	93
4	4.7	12.0	156
5B	5.7	11.3	98

Table 3.5. Average improvement in q_t using a geometric mean approach for the liquefiable soil layer in each zone for depths of 3.3 m to 11 m (255 days following installation)

Zone #	Average Corrected Tip Resistance Pre-treatment (MPa)	Average Corrected Tip Resistance Post-treatment (MPa)	Average Δq_t (%)
1	4.9	6.1	27
2	5.0	12.3	147
3	5.3	6.9	31
4	4.7	10.5	124
5A	5.3	13.1	147
5B	5.7	7.2	27

In the previous section a lack of improvement was observed between the 115-day and 255-day CPT soundings. This trend is also observed in Tables 3.4 and 3.5, where the average change in q_t decreased by approximately 30 to 70 percent between 10-day and 255-day soundings depending on the pile spacing and presence of drainage elements. It is hypothesized that the reduction in q_t was associated with a reduction in the lateral effective stresses, as "locked-in" compaction stresses generated during pile installation relaxed, similar to observations of mechanically compacted fill (Terzaghi et al. 1996). While the installation of piles is not similar to the placement and compaction of soil lifts, it is possible that the soil relaxes over time in a similar manner. Following installation, the soil density and ratio of horizontal and vertical effective stresses, *K*, initially increased. With time, the corrected cone tip penetration resistance decreased (Table 3.5). Since the vertical effective stresses could not change, the reduction in q_t may be attributed to the relaxation of horizontal effective stresses.

In order to evaluate the potential for relaxation, *K* was calculated for the pre- and post-installation conditions. The coefficient of earth pressure was estimated by setting the D_r obtained using each CPT sounding equal to a semi-empirical critical state CPT-based correlation proposed by Salgado and Prezzi (2007), and back-calculating the lateral effective stress and then computing *K*. This procedure was performed for each zone for the pre- and post-installation soundings with time every meter between 4 and 9 m below grade to evaluate the lateral stresses in the clean to silty sands in the

liquefiable zone, shown in Figure 3.35. In general, *K* was the largest just following pile installation; then, it appeared to decrease between the 10-day and 49-day soundings. Additional reductions were observed between 49 and 255 days, except for Zone 4, where *K* was larger during the 255-day sounding compared to the 49-day sounding, but still less than the 10-day *K* values. Differences are likely due to deviations between the planned and installed pile installation and spatial variability of the soil. Figure 3.35 shows the importance of time on the relaxation of horizontal stresses as measured using the cone tip resistance.

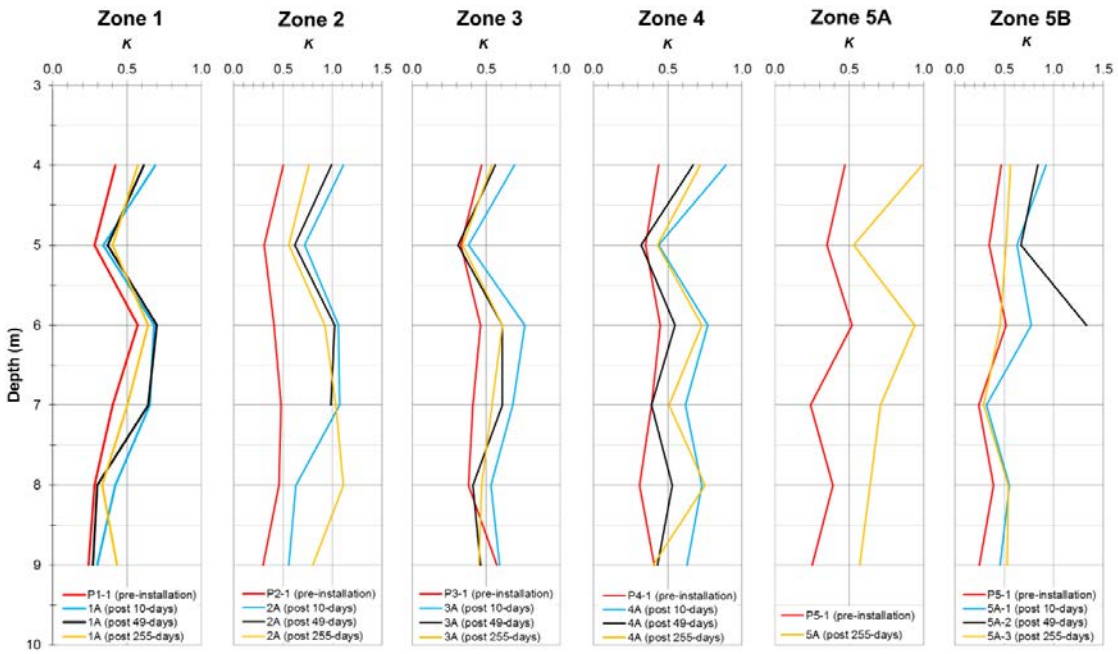

FIGURE 3.35 Change in coefficient of lateral earth pressure, *K*, for Zones 1 through 5 with time.

3.4 Controlled Blasting to Evaluate Pore Pressure Response and Post-Blasting Settlement

Controlled blasting has been implemented in research studies over the past 15 years to test the effectiveness of various ground improvement methods. Since the occurrence of earthquakes cannot be predicted with sufficient accuracy, controlled blasting allows researchers to model liquefaction for the evaluation of soil-foundation interaction at full scale. Ashford et al. (2000a, b), Ashford et al. (2004), Rollins et al. (2004), and Eller and Ashford (2011) have led advances in the use of controlled blasting to induce liquefaction and these studies served as guidance for the work described herein. When explosives are detonated they generate energy and initially create compressive stress waves throughout the soil followed by shear waves upon unloading. The use of multiple blasts, with delays between successive blasts, can be designed to load the ground in a cyclical manner, grossly similar, but not identical to earthquake ground motions. These cyclic ground motions and the corresponding shear stresses generate excess pore water pressures, and a soil may be considered to have liquefied when the pore pressure ratio, r_u reaches ~0.95 to 1.0, where r_u is the ratio of the pore pressure in excess of hydrostatic (u_e) and the vertical effective stress, σ'_{vo}. Controlled blasting to generate these excess

pore pressures allows for an assessment of the effectiveness of liquefaction mitigation when compared to an identical blast sequence conducted on unimproved ground.

A controlled blasting test program was planned to compare the unimproved (control zone) and improved (Zones 1–4) ground using conventional and drained timber piles. Zones 5A and 5B were not evaluated in the controlled blasting trial, as the as-built configuration of these zones would have resulted in necessarily complicated interpretation of the observed pore pressures. Pore pressure transducers (PPTs) were installed near the center of each zone in order to make one-to-one comparisons of pore pressure response. Ground surface elevation surveys were conducted to compare post-blasting settlements associated with pore pressure dissipation and reconsolidation. The PPT calibration and installation, explosive casing installation, explosive installation, and detonation sequence are discussed in detail in the following sections. Specific results from the blast-induced liquefaction program are also analyzed, and comparisons between Zones 1–4 are made to quantify the effect of pile spacing and presence of PVDs at mitigating liquefaction.

3.4.1 Experimental Details for the Controlled Blasting Program

Based on blast-induced liquefaction experiments performed by Rollins et al. (2005) it was determined that a pore pressure sensor should be able to withstand transient blast pressures and also measure residual pore pressures of ±0.69 kPa. With guidance developed from these earlier evaluations, Druck UNIK 5000 PPTs, model number A5034-TA-A3-CA-HO-PF, were selected for use during blasting. The PPT is an amplified pressure transducer capable of measuring pressure between 0 and 5.2 MPa, and withstand blast pressures of up to 20.7 MPa. Nineteen PPTs, distributed in five boreholes, were used to measure the pore water pressure during blasting. Prior to installation, the PPTs were individually calibrated as described in detail by Gianella (2015).

To help protect the PPTs, each PPT was housed in an acrylic case approximately 20 cm in length with an outside diameter of about 5 cm (Figure 3.36). The wall thickness of the housing was 0.6 cm. Each PPT was oriented vertically inside the housing with the tip located at approximately three-quarters of the length of the casing positioned at the elevation of the sintered bronze filters, as shown in Figure 3.36. Before attaching the filters to the housing in the field, they were boiled for approximately one hour to completely saturate and remove air from the voids. Thereafter, the filters were transferred to a water-filled container for assembly. Before connecting the filters to the sensor housing, each PPT housing was inspected for air bubbles and air bubbles were removed if found. The filters were then connected to the housing under water using set screws, and the housing prepared for installation.

Borehole B-1 in the center of the control zone and borings B-3, B-5, B-7, B-9 corresponding to the centers of Zones 1 through 4 in Figure 3.17(a), were drilled to facilitate installation of the piezometer strings. Split-spoon sampling was performed to 13.7 m for Zones 1 through 4 as shown in Figure 3.28. The borings were backfilled with sand to a depth of

9.14 m prior to placing the PPTs and housings. The four PPTs comprising each piezometer string were then carefully transferred to the borehole with a membrane to maintain saturation (*n.b.*, the membrane was removed in the borehole underwater), and individually lowered to the desired nominal depths (i.e., 9.14 m, 7.62 m, 6.10 m, and 4.57 m). Zone 3 was instrumented with just three PPTs owing to a manufacturing defect that was identified during calibration. Weights were connected with metal wire to the top cap to help the weighted PPT housings overcome buoyancy reach their desired depth. Cement-bentonite grout was then tremied to the base of each borehole to complete the piezometer string installation.

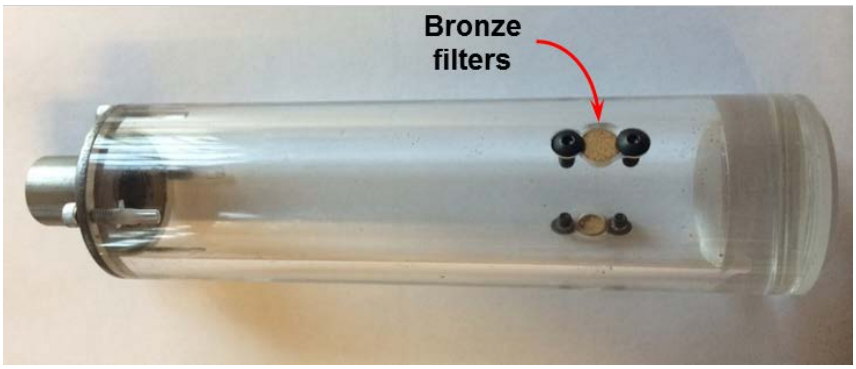

FIGURE 3.36 Photo of weighted acrylic PPT housing with metal cap and bronze filters.

3.4.2 Controlled Blasting of the Control Zone

The blasting program for the control zone consisted of four separate blasts, of which several were used to check the responsiveness of the PPTs and data acquisition system; however, this report focuses on the third and fourth blast events for brevity. Explosive charges were made using Pentaerythritol tetranitrate (PETN), sized to an equivalent of 0.91 kg of trinitrotoluene (TNT) and placed within blast casings. The third and main blasting event (termed BE3) at the control zone consisted of six blast casings designated B-1E2 through B-6E2 installed within a circular arrangement (with radius of 3.81 m) as shown in Figures 3.37 and 3.38, with four decks of charges in each casing. The decks were located at depths of 3.7 m, 5.3 m, 7.2 m, and 8.8 m below grade. Each of the 24 explosive charges contained an equivalent of 0.91 kg of

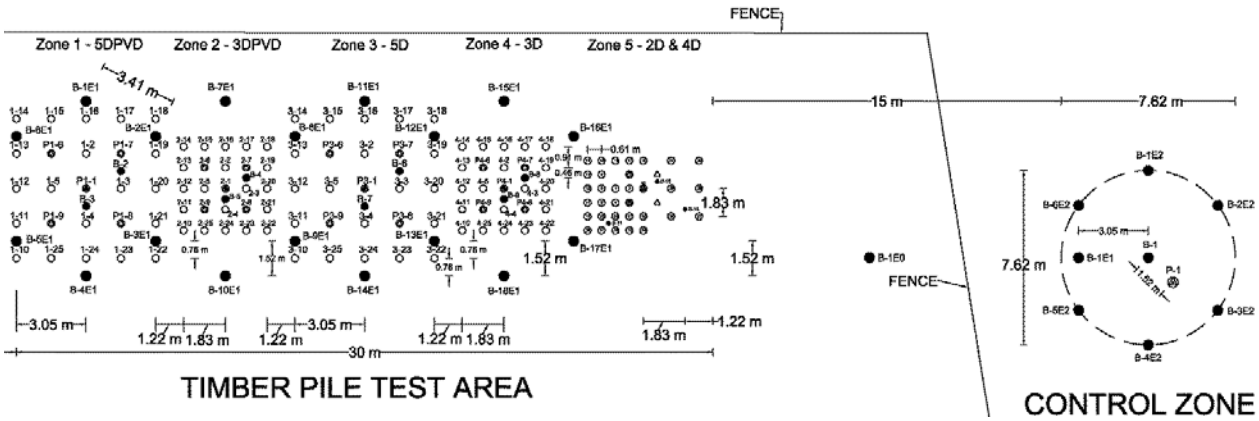

FIGURE 3.37 Site layout including pile locations, initial in situ tests, and explosive locations (blast casings are designated using "E"; e.g., B-1E1 and B-6E2, etc.)

TNT resulting in a total charge weight of 21.8 kg. This charge weight was selected based on the subsurface conditions from in situ tests at the test site and previous blast-induced liquefaction studies for the Cooper River Bridge in Charleston, South Carolina, reported by Camp et al. (2008). The intention was to verify that the charge weight necessary for liquefaction was correct prior to blasting the treated area.

The sequence of the 24 - 0.91 kg charges for BE3 was designed to create a rough analog to a cyclic motion. The blast sequence started at the bottom deck (i.e., at an elevation of 8.8 m below grade) and worked upwards toward the surface. The order of detonation is shown in Figure 3.38(b): detonation began at location #1, then proceeded to location #2, then two charges were detonated simultaneously at each location #3, followed by simultaneous detonations at each location #4. The charges were detonated sequentially from the bottom up with delays of 600 milliseconds between each explosion. After the detonation at each location #4, the cycle reset starting at location #1 at the next deck towards the surface. The total blast sequence was completed after 9 seconds. A photo of the control zone before blasting is shown in Figure 3.39.

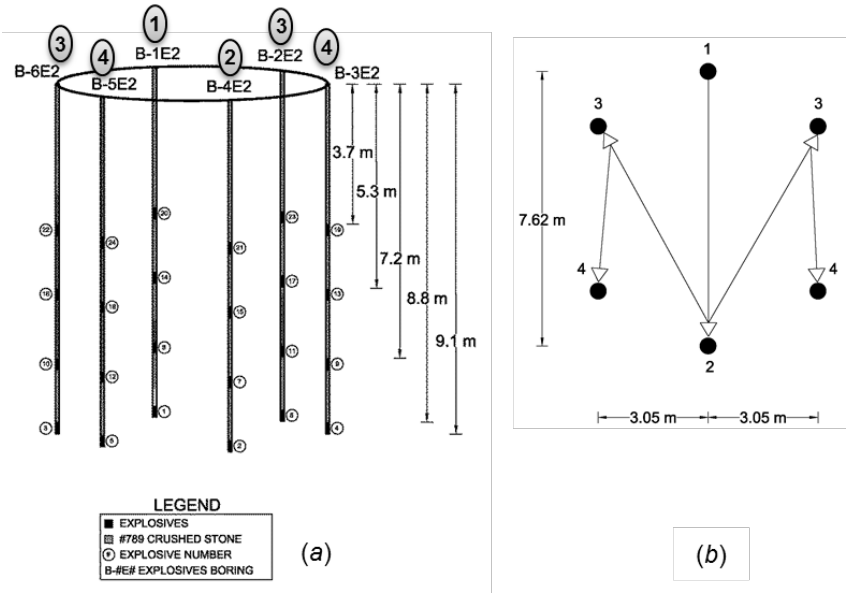

FIGURE 3.38 Controlled blast program and sequence in the control zone: (***a***) profile view indicating depths of explosive decks, and (***b***) plan view indicating blast sequence for each deck [compare sequence number in (***b***) to bubble numbers in (***a***)].

FIGURE 3.39 Control zone prior to blasting.

Concrete blocks were placed over each blast casing and tied down to stakes to prevent the explosives from detonating above their designed elevations as a result of the upward component of directed blast energy. Unfortunately, BE3 was unable to be executed using the intended 600 millisecond delay and timing of explosives. The 24 charges were performed over a relatively short time frame (i.e., approximately 1 second rather than the designed 9 seconds). It was important that the same blasting sequence and time of shaking for the control zone and the treated area were equal in order to make one-to-one comparisons. Therefore, new blast casings were installed in the control zone, and another attempt to blast the control zone was performed (i.e., BE4). Blasting event 4 was conducted correctly and a similar sequence was applied to the treated area. Although the desired sequence was not executed, the results of BE3 are described along with BE4.

Figures 3.40 and 3.41 show the excess pore pressure ratio time history for each of the PPTs measured during BE3 in the control zone. The PPTs at elevations of 6.35 m, 7.39 m, and 8.60 m reached peak r_u values of 126, 140, and 152 percent, respectively. Figure 3.41 shows an expanded view of Figure 3.40 which indicates that peak residual values ranged between 75 and 100 percent for approximately two minutes. This response indicates that complete liquefaction was achieved at the deepest elevation (i.e., r_u = 95 to 100%), and that near-complete liquefaction was achieved for the depth of 7.39 m. A large drop in pressure was observed at the shallowest location at approximately 10 seconds after blasting. This behavior indicates that water, and hence pore pressure, may have been able to escape quickly through cracks or fissures in the fill near the surface and relieve the high pressure. At approximately three minutes after blasting, r_u increased, and exhibited a similar dissipation rate as the other PPTs.

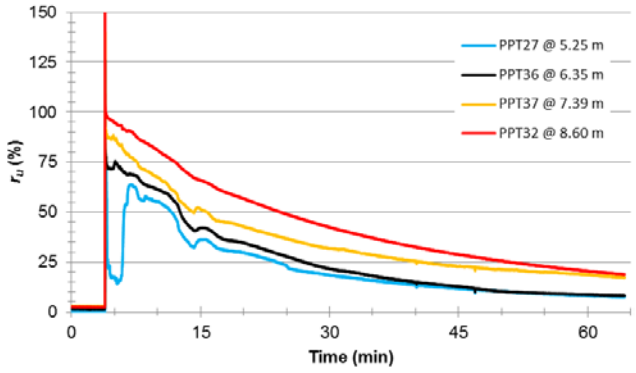

FIGURE 3.40 Dissipation of pore pressure after event BE3 in the control zone.

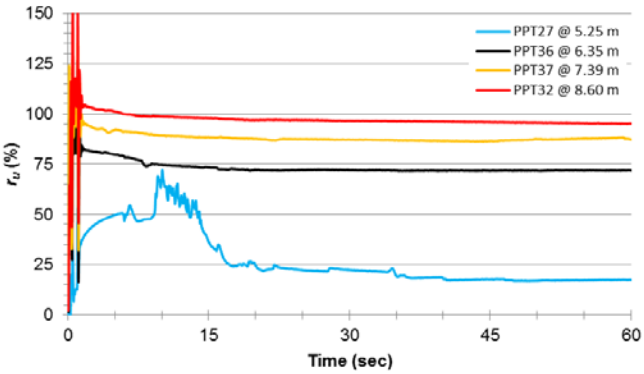

FIGURE 3.41 Expanded view of the dissipation of pore pressure after event BE3 in the control zone.

Blast event 4 was conducted using the 600 millisecond time delay similar to the sequence that was applied to the treated area. Figure 3.42 shows the generation of excess pore water pressure ratios for each PPT during the first 15 seconds. Each of the 16 individual detonations resulted in small peaks in r_u in this figure between 0.5 and 9.5 seconds. The shallowest PPT exhibited a delayed pore pressure response where peak r_u values were reached approximately 4 seconds after blasting was initiated as a result of the charges being detonated in the deepest decks first. All of the PPTs demonstrated a contractive soil response, indicating that soil in the control zone consisted of loose to medium dense, liquefiable sand. The PPTs at elevations of 5.06 m, 6.32 m, 8.02 m, and 8.58 m reached peak r_u values of 105, 147, 133,

and 148 percent, respectively. The two deepest PPTs exhibited complete liquefaction with peak residual values ranging from 95 to 105 percent. The peak residual values in the two shallow sensors ranged from 75 to 85 percent. Figure 3.43 shows the generation and dissipation of r_u for each of the PPTs for approximately 15 minutes following blasting. The r_u values decreased to less than 50 percent within 10 minutes following blasting except in the deepest PPT where r_u was approximately 60 percent at this time. In general, BE4 resulted in absolute increases in r_u values of approximately 10 to 20 percent compared to the single blast BE3. Sand boils were not observed in the control zone after blasting. Based on the site conditions the fill in the top 2.5 m of the site over the liquefied zone may have been too thick or impermeable, and served to prevent sand boils from occurring.

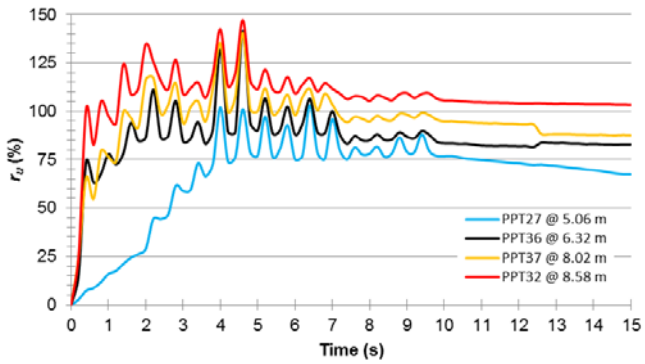

FIGURE 3.42 Generation of pore pressure during blasting event BE4 of the control zone.

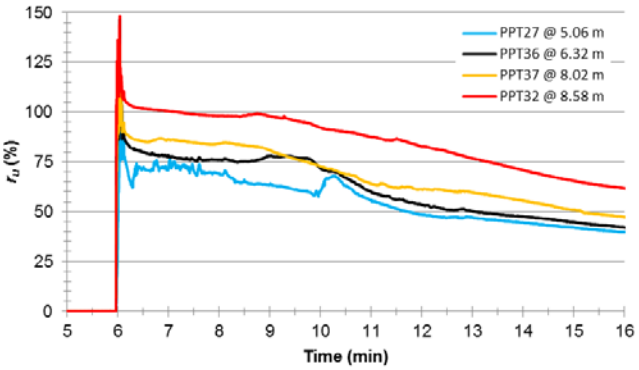

FIGURE 3.43 Dissipation of pore pressure after event BE4 in the control zone.

3.4.3 Post-blasting Settlement of the Control Zone

The ground surface settlement resulting from the controlled blasting following post-liquefaction consolidation was measured using an automatic level and rod. A baseline survey was performed prior to blasting at 29 individual points. These survey locations were made on three lines designated the A-line, B-line, and C-line as shown in Figure 3.44. Each line was spaced 60 degrees apart with the survey points spaced at 1.52 m intervals from the center of the control zone. Precautions were followed to ensure that the points could be re-established following each blast event, and so that the benchmark would be uninfluenced by the blasting. Ground surface elevations were surveyed approximately 3 and 20 hours after BE3. After three hours, r_u values ranged from 2 percent in the shallow PPTs to 4 percent in the deeper PPTs. The elevations were surveyed again the following morning to determine if any additional settlement occurred. On average, approximately 8 mm of additional settlement occurred between the 3- and 20-hour settlement surveys. Figure 3.45 presents the ground surface settlements for the three survey lines after 20 hours, and indicates that the maximum settlement, equal to about 160 mm, occurred in the center of the control zone and decreased with increasing distance from the center of the control zone. Another survey was performed along the A, B, and C-lines (Figure 3.45) 24 hours after BE4 and using the intended timing and delay sequence. The ground surface settlements measured along these lines indicate the differences in settlement between events with significantly different durations. The settlements observed

following BE4 were approximately 25 mm larger, on average, than those measured from BE3, and a maximum settlement of approximately 200 mm was observed near the center. An additional survey was performed 48-hours following BE4, but little to no additional settlement occurred. The cumulative settlement of the both blasting events is also shown in Figure 3.45 for each survey line, and indicates that the cumulative settlement equaled approximately 350 mm in the center of the control zone.

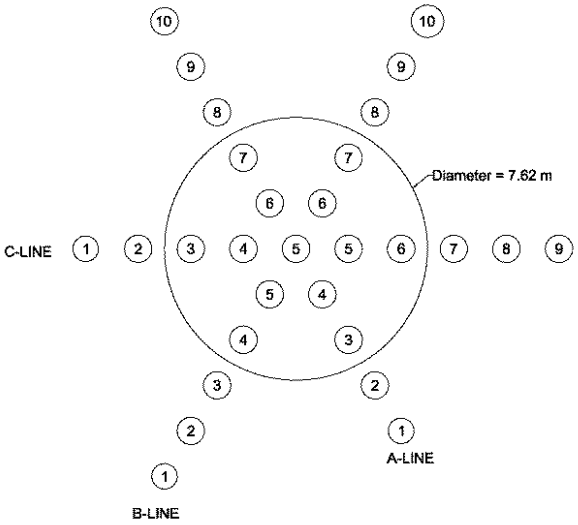

FIGURE 3.44 Layout of survey points to measure settlement in the control zone after blasting.

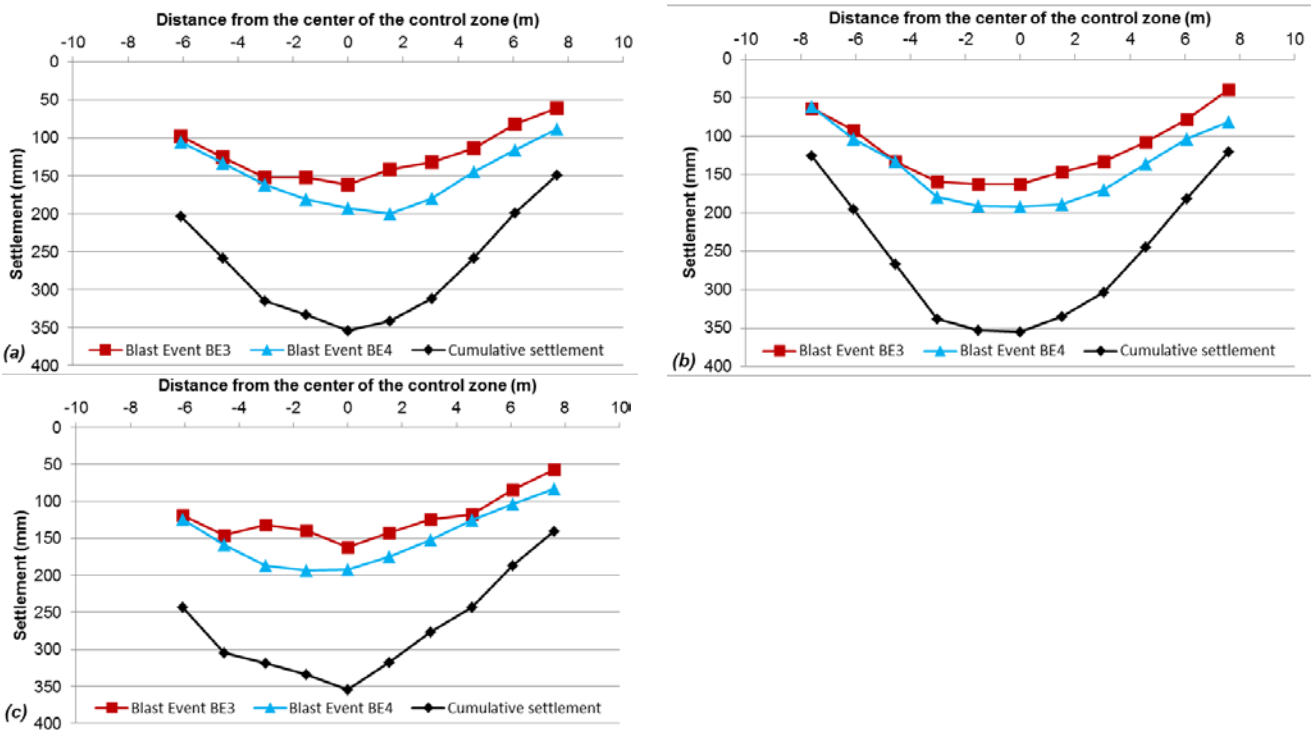

FIGURE 3.45 Ground surface settlement observed at the control zone comparing blasting events BE3 and BE4 for the (***a***) A-line, (***b***) B-line, and (***c***) C-line.

3.4.4 Controlled Blasting of the Treated Zones

Complete liquefaction was achieved with the designed charge weight and blasting sequence in the deepest portions of the liquefiable zone, and near-complete liquefaction was achieved for the shallow PPTs in the control zone. Based on these results, the same charge weight and blasting sequence was applied to the treated zones. The objective of blasting in the treated zones was to analyze the effectiveness of reducing pore pressures and mitigating liquefaction of the susceptible soils across the various treatment variables (i.e., the effect of pile spacing and presence of PVDs). The blasting program for the treated zones consisted of one blasting event, similar to the BE4 protocol; a plan and profile view of the blast casing distribution is shown in Figures 3.37 and 3.38. The blasting program of the treated zones consisted of 18 blast casings with four decks per casing located at the same elevations as those for the control zone. Each of the 72 explosive charges contained an equivalent of 0.91 kg of TNT resulting in a total charge weight of 65.5 kg. The blasting design consisted of the same blasting layout used in the control zone with each blast casing centered around Zones 1 through 4. A photo of the treated area prior to blasting is shown in Figure 3.46; concrete blocks were again used to cover each blast casing. The sequence of the 72 charges for the blasting event was generated to reproduce the energy created in the control zone by detonating the charges in a similar order as that of the control zone. The sequence was comparable to Figure 3.38, but not identical due to a larger number of charges being present with each zone adjacent to the other. The order of detonation in each deck is shown in Figure 3.47. As shown in this figure, the first blast consisted of four charges detonated simultaneously at each location #1, then four charges were detonated simultaneously at each location #2, then five charges were detonated concurrently at each location #3, followed by simultaneous detonations at each location #4. The charges are detonated sequentially with delays of 600 milliseconds between each detonation. Following the detonation at locations #4, the process restarted at the next deepest deck until all four decks were detonated, a process that lasted 9 seconds.

FIGURE 3.46 Treated zone prior to blasting.

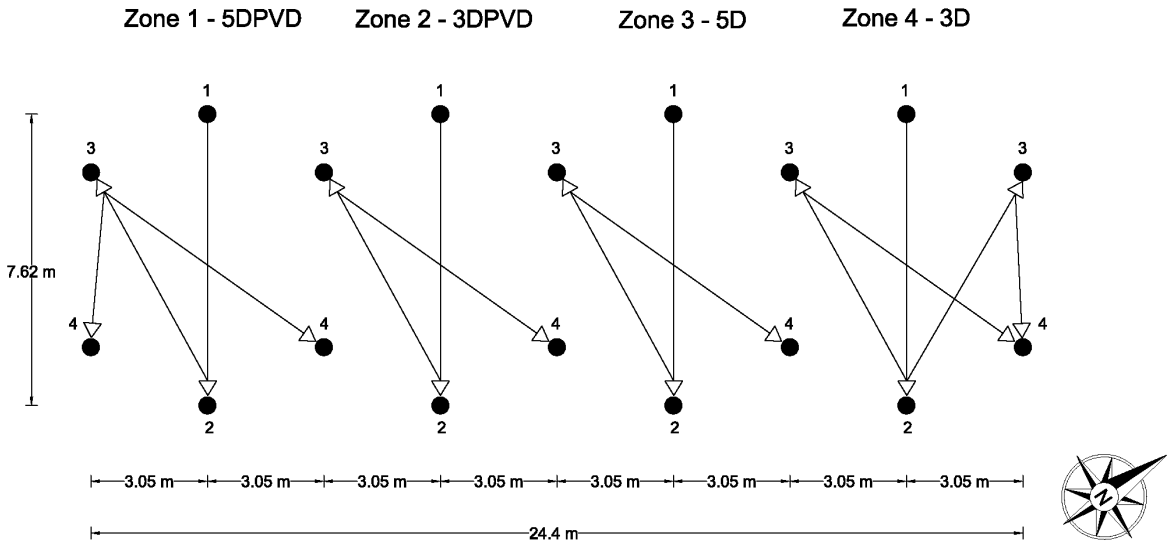

FIGURE 3.47 Blast sequence for each deck in the timber pile-improved area.

Figure 3.48 compares the generation of excess pore pressures in the treated zones at nominal PPT depths of 4.57, 6.10, 7.62, and 9.14 m to those observed in the control zone. In general, the pore pressure responses are similar between the treated zones. The bottom three PPTs (i.e., those at 6.10, 7.62, and 9.14 m) in each zone demonstrated a contractive soil response until approximately seven seconds, at which point a dilative soil response was observed (exhibited by a reduction in excess pore pressure at the instant of charge detonation). These PPTs recorded peak residual values ranging from approximately 75 to 85 percent with slight differences observed between zones based on pile spacing. The effect of dilative and contractive soil behavior during blasting is clearly shown in the shallow generation curves comparing the control zone and treated zones in Figure 3.48(a). The shallow PPTs (located at approximately 4.57 m depth) in each zone exhibited a dilative soil response shown by the larger troughs, or reductions, in excess pore pressure for each blast pulse. The peak residual values for these shallow PPTs ranged from approximately 55 to 65 percent. This indicates that the densified soil was much denser than the soils in the control zone at the same depth, where a contractive response was observed (Figures 3.42 and 3.48). All of the PPTs indicated excess pore pressures that were well below the complete liquefaction baseline of r_u = 95 to 100 percent, demonstrating that liquefaction was mitigated in all of the improved zones. The settlement response observed in the treated zones, discussed below, provides confirmation of the laboratory-based observations reported by Lee and Albaisa (1974) and Seed et al. (1975), where substantially larger magnitudes of r_u in dense soils can be allowed for a given level of allowable post-liquefaction reconsolidation settlement.

In order to make direct comparisons between the improved zones and un-improved control zone the peak residual pore pressures were selected at a time of 12 seconds (i.e., approximately three seconds after the last blast) and presented in Table 3.6. In general, all of the improved zones exhibited lower r_u values than the control zone, with the greatest absolute reduction of approximately 20 percent observed at the deepest PPTs as shown in Figure 3.48(d). The PPTs at 4.57 and 7.62 m showed a decrease in r_u of approximately 10 percent. There was no distinct trend between the drained

piles and the conventional piles, but the two uppermost PPTs in Zones 2 and 4 at 3*D* pile spacing had peak residual values of approximately 5 to 10 percent lower than those observed in Zones 1 and 3 at 5*D* pile spacing.

Table 3.6. Comparison of peak residual r_u values at 12 seconds

Nominal PPT depth (m)	r_u (%)				
	Control Zone	Zone 1	Zone 2	Zone 3	Zone 4
4.57	73	60	61	70	56
6.10	82	84	77	82	78
7.62	93	84	80	82	81
9.14	104	87	82	-	85

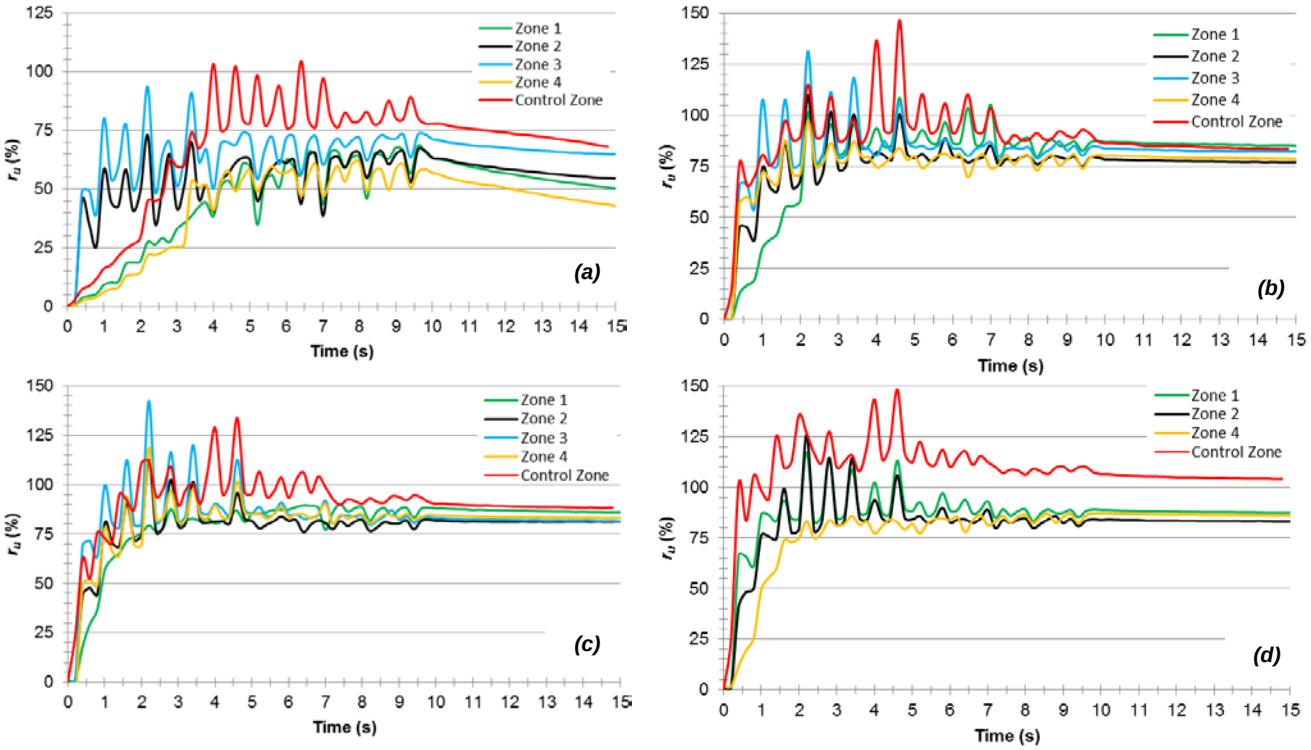

FIGURE 3.48 Comparing the pore pressure response of the treated zones to the control zone for (***a***) PPTs at a nominal depth of 4.57 m, (***b***) 6.10 m, (***c***) 7.62 m, and (***d***) 9.14 m. Note the transition from contractive to dilative pore pressure response in the treated zones with cumulative detonations.

3.4.5 Post-blasting Settlement of the Treated Zones

A ground surface survey was conducted to compare settlements in the treated zones to those in the unimproved control zone. A baseline survey was performed using the same automatic level and rod used for the control zone survey prior to blasting. These survey locations were set in a large square grid spaced at 1.52 m. A few piles in each zone were also observed so as to make comparisons among those piles that could not be driven to bear on the dense layers to those that could. The ground surface and pile heads were surveyed 24 hours following blasting, and the ground surface data used to generate the settlement contour plot shown in Figure 3.49. The settlement in the treated zones ranged from a minimum of 3 mm to a maximum of 99 mm; in general, the settlements equaled approximately one-quarter to one-third of those

observed at the control zone. The settlement response confirms the observations by Lee and Albaisa (1974) and Seed et al. (1975): soils with relative density in the range of 70 to 85 percent, such as those densified using the driven timber piles, will experience a much smaller increase in compressibility, as shown in Figure 3.50, and therefore smaller post-liquefaction reconsolidation settlement. Therefore, designers of densification-based ground improvement can allow larger in-shaking magnitudes of r_u. The piles that were not tipped into the dense sand layer at approximately 12.5 m below grade exhibited similar settlements as the surrounding soils, with settlements ranging from 54 to 97 mm. Adjacent piles that were embedded in the dense bearing layer exhibited much lower settlements, ranging from 0 to 46 mm, but equaled approximately 6 mm on average. Some piles appeared to heave (maximum heave of 25 mm observed), but this response represents an outcome of the blasting, and would not likely occur during a true earthquake.

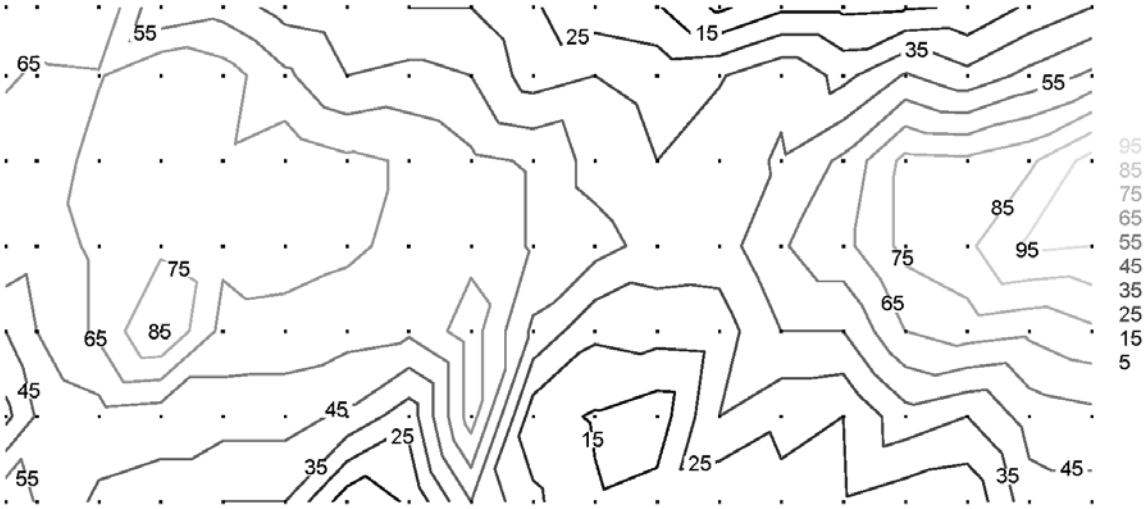

FIGURE 3.49 Settlement contours of the treated zones following blasting.

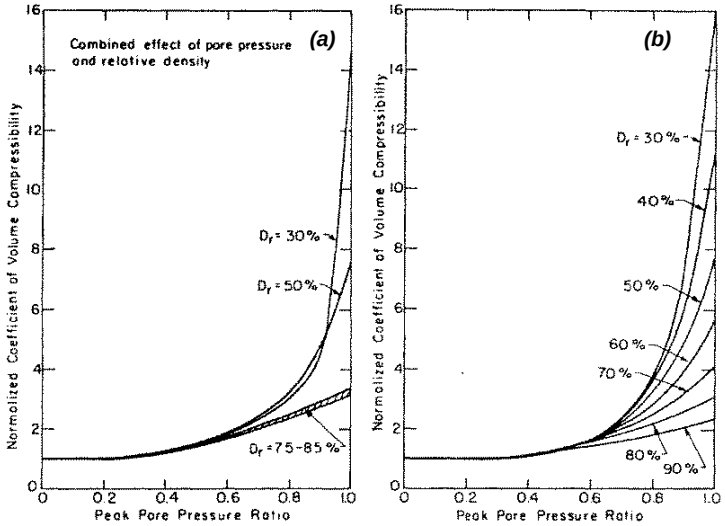

FIGURE 3.50 Relationship between peak excess pore pressure and soil compressibility: (***a***) after Lee and Albaisa 1974, and (***b***) after Seed et al. 1975.

3.5 Numerical Simulation of Controlled Blasting and Dissipation of Excess Pore Pressures

A coupled fluid-mechanical finite element (FE) model, FEQDrain, developed by Pestana et al. (1997) for use with earthquake drains, was used to simulate the observed pore pressure response. A FE model was generated and calibrated using the observed in situ conditions and the measured pore water pressure dissipation following blasting at the control zone. The calibrated model is then used to simulate the pore pressure response of the timber pile-improved zones. For brevity, the reader is referred to Pestana et al. (1997) for the theory employed by the finite element model, and Gianella (2015) for a detailed description of the model calibration.

There are four cases that can be modeled using the FEQDrain program: an untreated condition (i.e., no drain), a perfect drain analysis exhibiting no drain resistance, an equivalent granular drain simulating a gravel drain (i.e., stone column), and a PVD (e.g., an earthquake drain). The first case is used for calibration of the FE model to the control zone since there are no drains present. This no-drain case was also used for the prediction of the conventional pile Zones 3 and 4. For the drained timber pile Zones 1 and 2, the response was predicted using the fourth case, considering the geometry and discharge parameters associated with the PVD used. The selection of input parameters for the control zone is described first, and the modification of the model parameters to account for the improved zones is described thereafter.

3.5.1 Numerical Simulation of the Control Zone

The soil profile at the control zone consisted of seven soil layers based on the site stratigraphy described earlier; relevant soil properties such as the hydraulic conductivity, relative density, and modulus of volume compressibility were required for modeling the generation and dissipation of the blast-induced excess pore pressures. The initial vertical hydraulic conductivity, k_v, for each soil layer was selected based on three representative soil samples (the same used to estimate relative density as described previously) and correlations to the grain size distributions developed from laboratory test analyses (Gianella 2015). Since the horizontal hydraulic conductivity, k_h, is typically larger than k_v as a result of the geologic deposition process, it was estimated by multiplying k_v by 1.5 and 4 for clean and silty sand layers, respectively. Numerous calibration trials were required to adjust the estimated k_h and k_v values until the pore pressure dissipation rate observed at each PPT was in agreement with the measured response. The selected hydraulic conductivities are shown for each soil layer in Table A1 of the Appendix, and all fall within typical values for sandy soils. The relative density for each of these soil layers in the control zone was selected based on the initial CPT-based relative density for P-1 as shown in Figure 3.16. The soil layer depths, saturated unit weights, γ_{sat}, and relative densities, D_r, are summarized in Table A1 of Appendix A. These parameters were not modified during calibration to the control zone. The initial coefficient of volumetric compressibility, m_{vo}, of the clean sand layers was set equal to 2 x 10^{-5} m^2/kN based on typical values for Sacramento River Sand (PHRI 1997). Bandini and Sathiskumar (2009) performed flexible wall permeameter tests on clean to silty sands with up to 25 percent *FC* and showed that m_v increases with increasing silt content. Values of m_v exhibited a linear trend from approximately 2 x 10^{-5} to 4 x 10^{-5} m^2/kN for 0 and 25 percent silt content, respectively.

Based on Bandini and Sathiskumar (2009), initial m_v values for the silty sand sample representative of the silty sand layers at the test site were set equal to 3.3 x 10^{-5} m^2/kN. However, it is noted that m_v depends on D_r and r_u as described earlier (Figure 3.50), and changes throughout shaking in FEQDrain at each time step. The m_{vo} values were not altered during calibration to the control zone.

The generation of excess pore pressure is directly related to the number of loading cycles, and this can be normalized by the number of cycles required to cause liquefaction, N_L. As N_L increases, the soil is more resistant to liquefaction, resulting in a lower r_u values for a given number of cycles. The cyclic resistance ratio (*CRR*) for each layer in the FE model was estimated using the Seed et al. (1985) triggering curves with corrected SPT penetration resistance, $N_{1,60}$ from boring B-1 and the observed fines content. After the *CRR* to induce liquefaction for each soil layer was determined, Figure A1 was used to determine N_L of each soil layer. Table A2 shows the average $N_{1,60}$ and *FC* used to estimate the *CRR* and N_L for the calibrated control zone model. The FE model simulates earthquake loading by the specification of the number of equivalent cycles, N_{eq}, and the duration, t_d, of an earthquake. Since a specific earthquake (e.g., magnitude, acceleration, etc.) was not modeled, N_{eq} and t_d were selected based on the blasting program implemented in the control zone: sixteen individual cycles (i.e., one per detonation) were applied over a 9 second time period. Each detonation was taken as an earthquake cycle (i.e., N_{eq} = 16) over t_d = 9 seconds for the FEQ simulation. It is of interest to note that the input earthquake parameters associated with the blasting program appear to correspond to an earthquake event with a magnitude ranging from 6.0 to 7.5 (based on Seed et al. 1975; Seed and Idriss 1982). The selected input parameters for the control zone FE model are summarized in Table A1. The FE model of the control zone was calibrated by adjusting k_h and k_v values, only, until the measured and computed pore pressure response was in agreement.

Figures 3.51 through 3.54 present the generation and dissipation of r_u in the control zone at depths of 5.06, 6.32, 8.02, and 8.58 m for BE4, along with the pore pressures computed using FEQDrain. The computed response using FEQDrain does not show peaks in r_u for each cycle as observed for each blast pulse measured in the field, but the peak residual values are similar at approximately 10 seconds once the detonations have ceased. Figures 3.51 through 3.54 also compare the measured and computed dissipation of r_u for 30 minutes following blasting, and indicate that the rate of dissipation was satisfactorily modeled. An additional simulation was performed using this FEQDrain model for a longer dissipation time history to allow the pore water pressures to dissipate to hydrostatic pressures in order to compare the measured and computed settlement. Following complete dissipation, the total settlement predicted equaled 178 mm, which compares favorably to the 200 mm maximum settlement measured in the center of the control zone following BE4.

3.5.2 Numerical Simulation of the Treated Zones

Following the calibration of a suitable FE model for the control zone, modeling of the treated zones could be accomplished reliably. The calibrated k_h and k_y values from the control zone were used to predict the pore pressure response

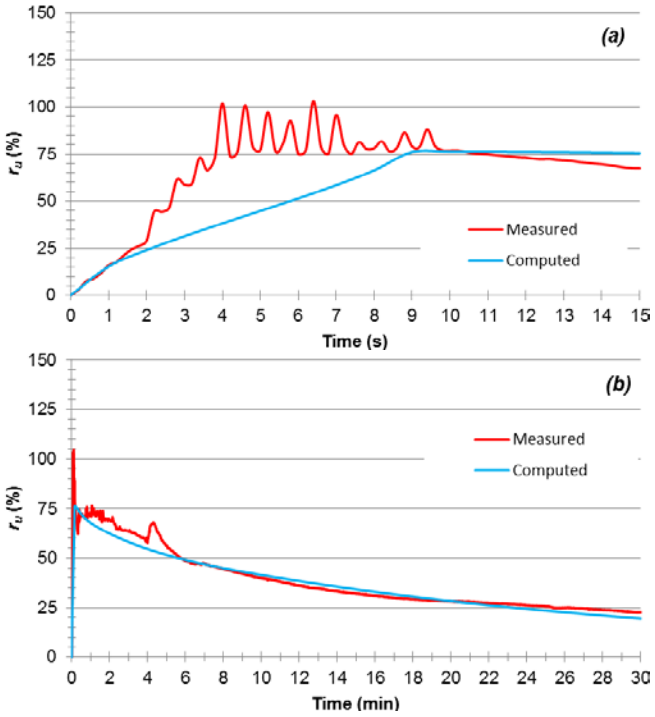

FIGURE 3.51 Comparison of measured and calculated excess pore pressure ratios in the control zone at a depth of 5.06 m, showing the (***a***) generation of excess pore pressure, and (***b***) dissipation of excess pore pressure.

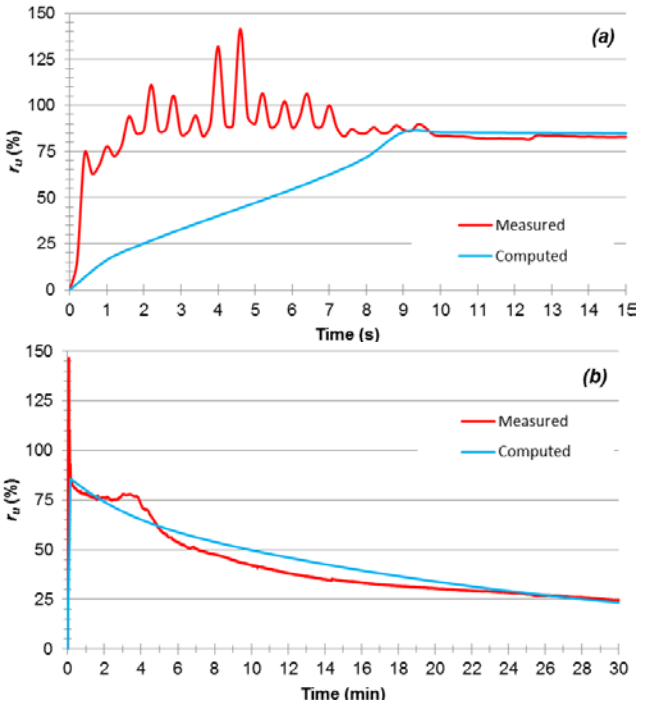

FIGURE 3.52 Comparison of measured and calculated excess pore pressure ratios in the control zone at a depth of 6.32 m, showing the (***a***) generation of excess pore pressure, and (***b***) dissipation of excess pore pressure.

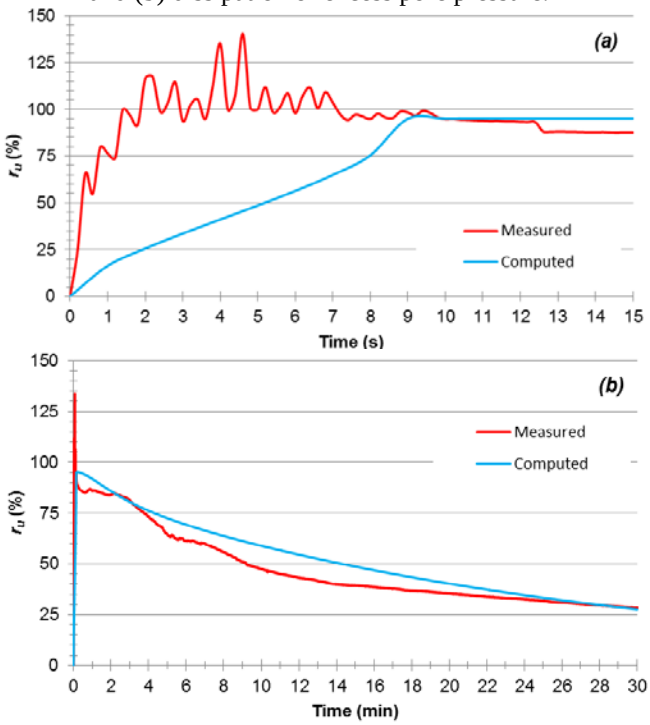

FIGURE 3.53 Comparison of measured and calculated excess pore pressure ratios in the control zone at a depth of 8.02 m, showing the (***a***) generation of excess pore pressure, and (***b***) dissipation of excess pore pressure.

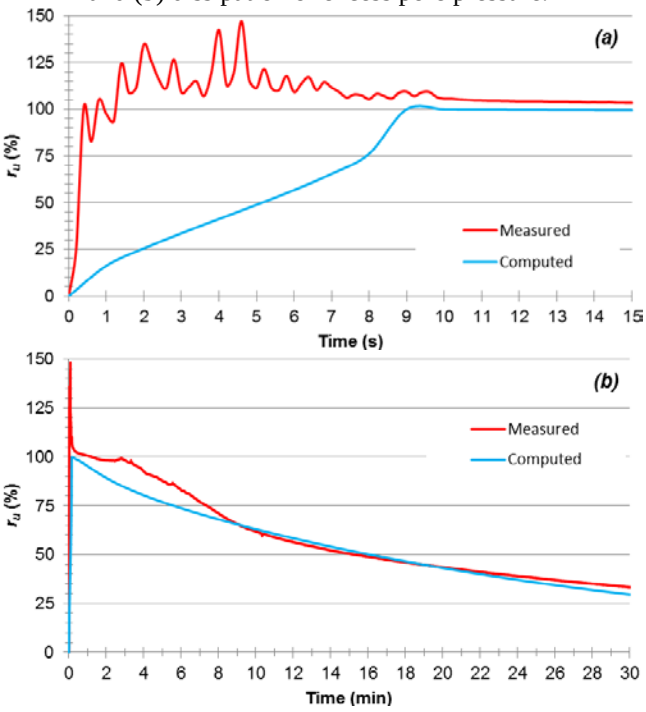

FIGURE 3.54 Comparison of measured and calculated excess pore pressure ratios in the control zone at a depth of 8.52 m, showing the (***a***) generation of excess pore pressure, and (***b***) dissipation of excess pore pressure.

in the treated zones. Following densification, these parameters, along with m_v, would be expected to decrease since the void ratio decreased; however, the magnitude of decrease was unknown, and it was decided to keep the initial values the same. Further research should be performed to evaluate changes in m_v, k_h, and k_v following densification. Since the settlement calculations in FEQDrain are based on m_v, it was decided that an appropriate settlement prediction could not be made for the treated zones. To reflect the ground improvement and improved cyclic resistance expected from the observed densification, D_r, $N_{L,}$ and γ_{sat} were updated using the 255-day CPT and SPT data. The same methods for the control zone described above were used to select the D_r, N_L, and *CRR* for each zone following timber pile installation. Tables A3 through A6 show the average $N_{1,60}$ and *FC* corresponding to borings, along with the post-installation *CRR* and N_L, for the improved Zones 1 through 4. For layers with *FC* between 0 and 15 percent *FC*, the post-installation N_L was determined by taking the average of two values obtained using Figure A1. The soil input properties for each zone are summarized in Tables A7 through A10.

The measured and computed generation and dissipation of excess pore pressures for Zones 3 and 4, representing timber pile-improved ground without drains, are shown in Figures 3.55 and 3.56, respectively. In general, the computed and measured responses were nearly identical for the majority of PPT observations, indicating that FEQDrain is capable of modeling the pore pressure response of timber pile-densified ground provided that the increase in relative density and cyclic resistance can be estimated reliably. The generation of excess pore pressure at the shallowest PPT [Figure 3.56(a)] in Zone 4 and the deepest PPT [Figure 3.55(c)] in Zone 3 were not as well modeled as the majority of PPT locations, and the measured r_u values for these observations were approximately 10 to 15 percent lower. The dissipation of residual pore pressures following generation in Figures 3.55(a) and 3.56(b) also exhibited lower r_u values than computed by FEQDrain. However, these deviations in excess pore pressure magnitude are on the conservative side, and the remainder of the observations appear suitably modeled given that the relative density and cyclic resistance ratios selected based on the post-installation in situ tests represent the only variables altered between these simulations and those of the control zone.

The driven timber piles fitted with PVDs in Zones 1 and 2 were modeled in FEQDrain as a vertical composite drain with perforations similar to the approach used for earthquake drains. The equivalent diameter of the PVDs implemented in the treated zones was calculated using the Hansbo (1979) equation expressed as:

$$d_e = \frac{2(a+b)}{\pi}$$

where a is the width of the PVD (equal to 100 mm), and b is the thickness of the PVD (equal to 4.3 mm). Only one width of drain was exposed on each side of the pile, and therefore the overall area of each drained pile was not modeled as twice the area of a single drain. Rather, the thickness was multiplied by 2 (i.e., b = 8.6 mm) in order to account for the use of a drain on each side of the PVD-wrapped pile. The equivalent diameter was used to calculate the effective storage area of the drain, a_{read}, by using the equation for a right cylinder. The equivalent radius and effective storage area of the drain,

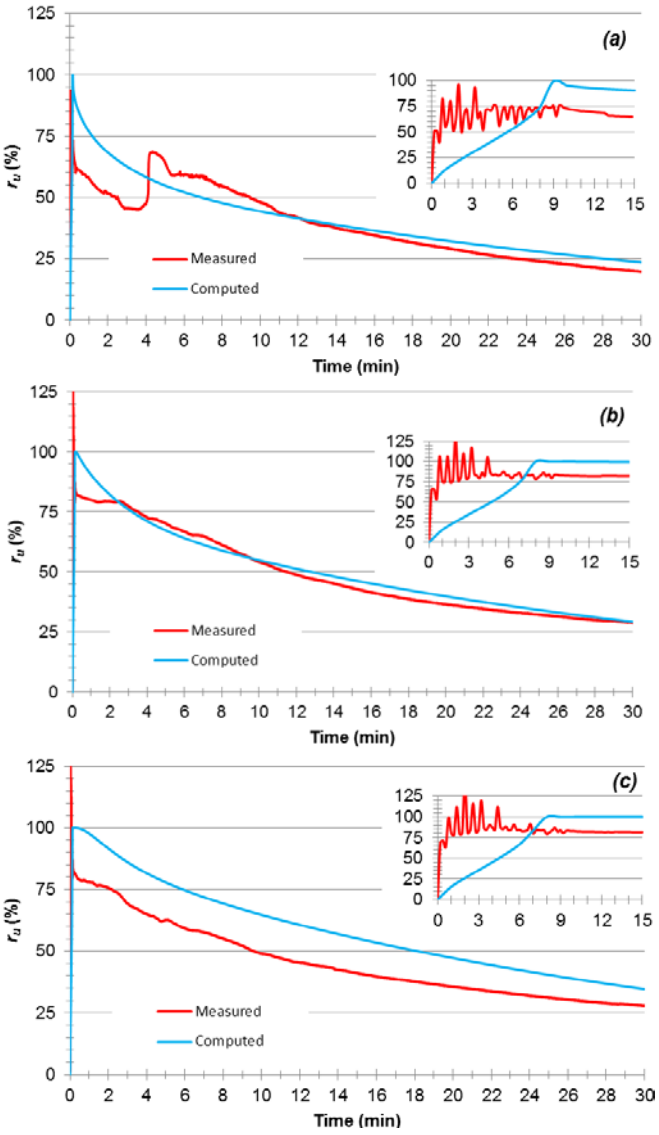

FIGURE 3.55 Comparison of measured and computed generation and dissipation of excess pore pressure ratios in Zone 3 at depths of (***a***) 4.83 m, (***b***) 6.08 m, and (***c***) 7.64 m. Inserts show initial 15 seconds of pore pressure time history.

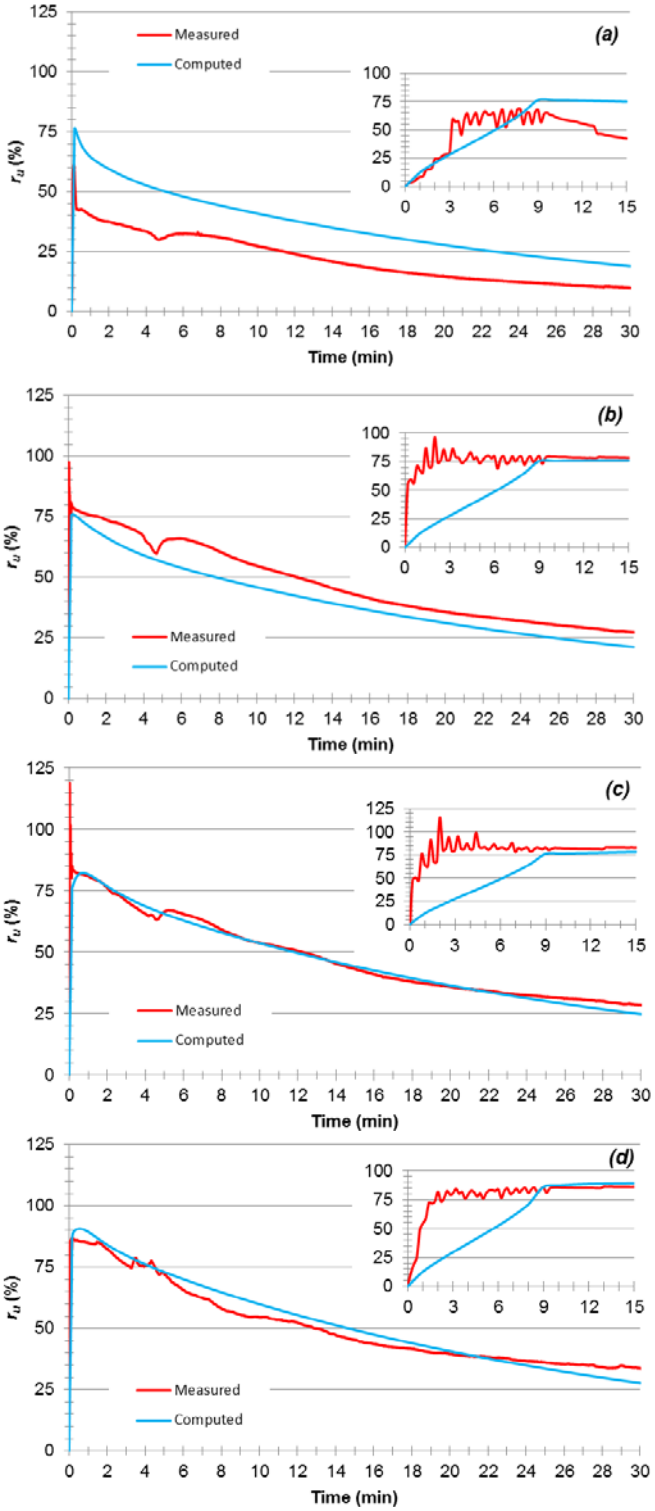

FIGURE 3.56 Comparison of measured and computed generation and dissipation of excess pore pressure ratios in Zone 4 at depths of (***a***) 5.39 m, (***b***) 6.07 m, (***c***) 7.44 m, and (***d***) 8.98 m. Inserts show initial 15 seconds of pore pressure time history.

r_w and a_{read}, that were used to compute the pore pressure response with the drained piles using FEQDrain are shown in Table 3.7, along with all of the other required model parameters. The permittivity and area of openings per unit length, *orf,* were selected using the manufacturer specifications for the MD-88 PVD drain used (Hayward Baker 2014), and presented in Table 3.1. The constant c_{orf} was set equal to 1.0 as a typical value representing standard head loss through the drain perforations. The effective storage area of the reservoir, a_{rear} was set equal to a_{read} and the depth of the reservoir, *depress* was set equal to 0 m. The only drain parameter that was different between Zones 1 and 2 was the radius of the tributary area from the drain, r_{out} which is a function of spacing. The equivalent radius, r_{out}, was calculated using the equation above for the square pile layout, and equal to 0.86 and 0.52 m, for Zone 1 and 2, respectively.

Figures 3.57 and 3.58 present the measured and computed generation and dissipation time histories of excess pore pressures for Zones 1 and 2, respectively. In general, the FEQDrain computations greatly over-predict the actual performance of the drained pile groups, with r_u over-estimated by approximately 30 to 65 percent compared to the measured data. The predicted excess pore pressure ratios in these figures correspond to dissipations at the drain (i.e., r = 0.0 m from the drain). To assess the measured response more accurately, a comparison was made to the computed pore pressures in the middle of two drained piles, (i.e., r = 0.75 m) for Zone 1. However, very little difference in the excess pore pressure generation or dissipation curves was computed (Gianella 2015). Based on these analyses, the FE model was not able to reproduce the measured response for the drained timber piles. Since the measured pore pressure response was similar for the conventional and drained timber pile zones, the drained timber pile prototype may not have provided sufficient discharge capacity to handle the excess pore pressures generated, or may have been pinched or damaged following the pile driving process preventing the PVDs from working over the long term. Further research could be performed to address these potential shortcomings.

Table 3.7. Summary of drain and reservoir input parameters used in FEQDrain simulations for Zones 1 and 2

Model Parameter	Value	Description
c_1	0	Material constant for vertical drain resistance
c_2	1	Material constant for vertical drain resistance
c_{orf}	1	Constant for head loss through pipe perforation
orf	0.065 m^2/m	Area of openings per unit length in perforated pipe
permit	0.3 sec^{-1}	Permittivity of fabric in composite drain
a_{read}	3.754 x 10^{-3} m^2	Effective storage area of drain
r_w	0.035 m	Well radius
a_{rear}	3.754 x 10^{-3} m^2	Effective storage area of the reservoir
depress	0.0 m	Depth below surface to bottom of reservoir
c_3	0	Material constant for vertical resistance in reservoir
c_4	1	Material constant for vertical resistance in reservoir

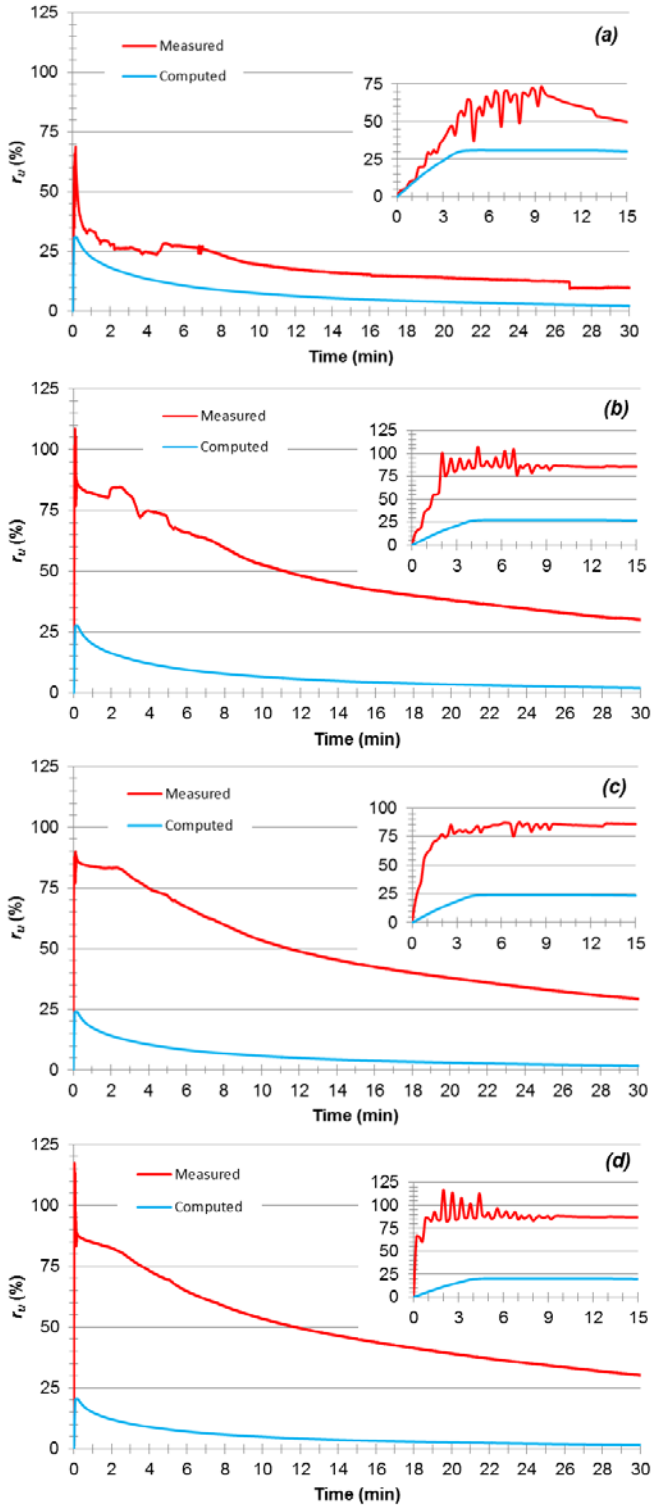

FIGURE 3.57 Comparison of measured and computed generation and dissipation of excess pore pressure ratios in Zone 1 at depths of (***a***) 5.06 m, (***b***) 6.07 m, (***c***) 7.42 m, and (***d***) 9.14 m. Inserts show initial 15 seconds of pore pressure time history.

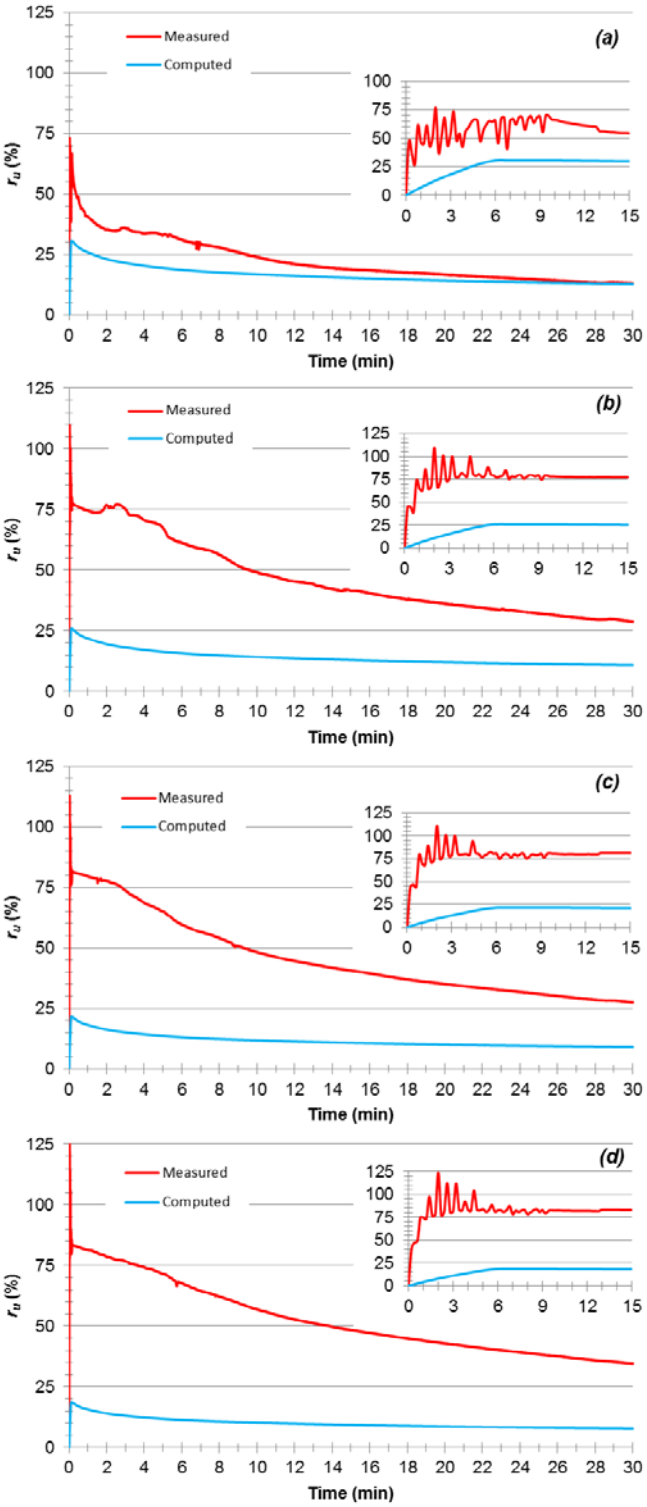

FIGURE 3.58 Comparison of measured and computed generation and dissipation of excess pore pressure ratios in Zone 2 at depths of (***a***) 4.95 m, (***b***) 6.13 m, (***c***) 7.53 m, and (***d***) 8.98 m. Inserts show initial 15 seconds of pore pressure time history.

4.0 PLANS FOR IMPLEMENTATION

4.1 Summary of Findings and Possible Improvements

The study herein focused on the evaluation of conventional and novel drained timber piles for the purpose of ground improvement through densification of liquefiable soil deposits and possible drainage during strong ground motion. The results of this study show that:

1. The relative density of liquefiable soils reached 60 to 95 percent (i.e., increase in relative density of 20 to 55 percent) immediately following installation of timber piles, depending on the pile spacing and use of pre-fabricated vertical drains (PVDs).
2. Long-term (i.e., at 255 days following installation) measurements of corrected cone tip resistance, q_t, showed that the increase in q_t equaled approximately 30 percent for piles spaced at four to five diameters, D, with and without PVDs, 125 percent for piles at 3D without PVDs, and about 145 percent for piles spaced at 3D with drains and 2D without drains. Therefore, it appears that drained piles were effective in improving the relative density relative to the conventional piles when the pile spacing was sufficiently close (3D). The closely spaced drained piles were shown to perform better in silty regions than the conventional piles.
3. Long-term measurements of corrected cone tip resistance measurements suggest that relaxation occurred in the densified ground following installation of driven timber piles; however, this phenomenon necessarily occurs at constant relative density.
4. Long-term standard penetration test-based N_{60} blow counts typically increased 5 to 20 blows per 0.3 m in the liquefiable soil layer depending on the pile spacing, as measured 292 days following pile installation.
5. Controlled blasting performed to develop a baseline for comparison to the improved ground indicated that the selected charge weight and pattern was able to produce complete liquefaction in the two deepest PPTs, and this charge pattern resulted in maximum settlements of about 200 mm in the center of the control zone.
6. Peak residual excess pore pressures as described using the excess pore pressure ratio, r_u, were reduced by absolute values of up to 22 percent in the timber pile-improved zones, thus preventing the triggering of liquefaction.
7. The drained timber pile zones exhibited similar reductions in r_u and dissipation rates as the conventional timber zones, suggesting that the drains did not provide sufficient discharge capacity to reduce excess pore pressures following controlled blasting.
8. The average settlements observed in the improved zones were approximately one quarter to one third of the settlement observed for the same charge sequence applied to the unimproved control zone.
9. Timber piles embedded in the dense sand layer had a median settlement of 6 mm compared to piles that were not toed-in the dense layer exhibited much larger settlements with a median settlement of 73 mm.
10. The finite element (FE) model prediction of generation and dissipation of excess pore pressures for conventional timber pile Zones 3 and 4 were generally in very good agreement. However, the FE model over-predicted the pore pressure reductions in the drained timber pile zones, with predicted r_u values approximately 30 to 65 percent lower than the measured in situ data.

The findings summarized above clearly point to the effectiveness of drained and conventional driven timber piles in densifying liquefiable soils and mitigating the effects of liquefaction (i.e., post-liquefaction settlements). Drained piles at relatively close spacing (i.e., 3*D*) produced improved densification and slightly lower blast-induced excess pore pressures than any other alternative. However, the potential to drain shaking-induced excess pore pressures during strong ground motions was not achieved with the drained piles owing to insufficient discharge capacity. Additional funds will be sought to improve the discharge capacity of drained piles.

4.2 Implementation of Findings

The implementation of this technology is best described through the lenses of the considerations for implementation, technology transfer, and possibility for the use of this technology at a demonstration project.

4.2.1 Considerations for Implementation

Briefly, prior to using this technology in the field, an owner should consider the following items.

- Considerations with regard to the findings presented here include:
  - The drained piles appeared to produce a benefit in densification at a pile head spacing of three diameters, but did not appear to provide a benefit at five pile head diameters spacing. This could be related to the length of the radial drainage path, which governs the rate and success of drainage.
  - A comparison of the improvement in relative density of driven, drained piles spaced at a pile head spacing of 3, 3.5, and 4 diameters would help to improve the resolution of findings presented herein.
  - Such an additional study could lead to optimization of densification, materials usage requirements, and cost.
- Considerations with regard to the design of conventional and drained timber piles include:
  - Specific design methodologies have not been developed for use with driven displacement piles.
  - Specific design methodologies developed for other technologies (e.g., deep soil mix columns, piled embankments) should be adapted for use with driven timber piles to account for densification and the flexural rigidity associated with timber materials.
  - New design methodologies need to focus on the seismic response of approach embankments, abutments, and bridge pier armoring (e.g., for liquefaction, lateral spread, etc.).

4.2.2 Technology Transfer

In order to assist in the implementation of this ground improvement alternative, the principal investigator will present findings to regional, national, and international audiences. Emphasis will be given to those conferences where state and federal highway officials will attend. For example, the principal investigator recently delivered (or will deliver) presentations at the following gatherings (to date):

- August 4, 2015: 40th Annual Northwest Geotechnical Workshop, Gleneden Beach, OR; attended by members of Alaska, Colorado, Idaho, Montana, North Dakota, Oregon, South Dakota, Utah, Washington, Wyoming DOTS and the FHWA
- September 3, 2015: 16th Annual Design and Installation of Cost-Efficient Piles Conference, Pile Driving Contractor's Association, Newark, NJ
- October 20, 2015: Korea Maritime and Ocean University, Busan, South Korea
- October 21, 2015: Korea University, Seoul, South Korea
- November 3, 2015: 6th Int. Conf. of Earthquake Geotechnical Engineering, Christchurch, New Zealand
- December 2, 2015: Offices of Hart Crowser, Inc., Beaverton, OR, and Seattle, WA
- December 2, 2015: Portland ASCE Geotechnical Group, Dinner Meeting, Lake Oswego, OR
- December 8, 2015: University of California, Los Angeles, CA
- February 16, 2016: ASCE GeoStructures Congress, Phoenix, AZ
- March 31, 2016: South Carolina PDCA Annual Conference, Charleston, SC
- April 1, 2016: Members of the South Carolina DOT, Columbia, SC

Additionally, this work will be published in conference proceedings and journal publications. In order to improve the exposure of this work, presentation of findings in a poster at the Annual Meeting of the Transportation Research Board in January 2017 will be sought.

4.2.3 Demonstration Project

The principal investigator has initiated discussions with several state and federal highway officials to investigate the possibility of implementing drained timber on state and federal bridge approach fills and abutments; such activities will lead to wider use of this technology. The demonstration project will attempt to leverage the demonstration funds available as part of the "Every Day Counts" initiative, and interested parties are encouraged to contact the Principal Investigator to seek collaboration on this effort.

4.3 Closing Statement

The summary of findings described above indicate that while additional work can be performed to improve the in-shaking performance of the drained timber pile prototype, *there are no barriers for the use of drained or conventional piles to densify liquefiable soils.* Because there is no proprietary information associated with this innovation, state departments of transportation and their design consultants may begin to implement this technology immediately. In those areas of the nation where both a plentiful supply of timber (e.g., Southern Pine and Douglas Fir) and seismic hazard exist, this technology will offer a "green" or sustainable ground improvement alternative, reducing the carbon footprint of construction as the costs associated with the nonrenewable mining and production of virgin aggregate and cement are avoided. Such alternatives are certain to gain wider acceptance over the coming years, particularly as this technology is demonstrated on public infrastructure projects.

5.0 REFERENCES

Andrus, R.D., R. Boller, W.M. Camp, S. Gassman, M. Hasek, H. Hayati, and P. Talwani (2008). "Characterizing the Liquefaction Resistance of Aged Soils: Summary of Selected First Year Findings," *Proceedings of NSF Engineering Research and Innovation Conference*.

Ashford, S.A., K.M. Rollins, and J.I. Baez (2000a). "Comparison of Deep Foundation Performance in Improved and Non-Improved Ground Using Blast-Induced Liquefaction," In *Soil Dynamics and Liquefaction 2000*, ASCE, Reston, Va., pp. 20–34.

Ashford, S.A., K.M. Rollins, V.S.C. Bradford, T.J. Weaver, and J.I. Baez (2000b). "Liquefaction Mitigation Using Stone Columns Around Deep Foundations: Full-Scale Test Results," *Transportation Research Record: Journal of the Transportation Research Board, No. 1736*, Transportation Research Board of the National Academies, Washington, D.C., pp. 110–118.

Ashford, S.A., K.M. Rollins, and J.D. Lane (2004). "Blast-Induced Liquefaction for Full-Scale Foundation Testing," *Journal of Geotechnical and Geoenvironmental Engineering*, ASCE, Reston, Va., Vol. 130, No. 8, pp. 798–806.

Bandini, P. and S. Sathiskumar (2009). "Effects of Silt Content and Void Ratio on the Saturated Hydraulic Conductivity and Compressibility of Sand-Silt Mixtures," *Journal of Geotechnical and Geoenvironmental Engineering*, Vol. 135, No. 12, pp. 1976–1980.

Boulanger, R.W. and I.M. Idriss (2014). *CPT and SPT Based Liquefaction Triggering Procedures*, Report UCD/CGM-14/01, Department of Civil and Environmental Engineering, University of California, Davis, 138 pp.

Camp, W.M., P.W. Mayne, and K.M. Rollins (2008). "Cone Penetration Testing Before, During, and After Blast-Induced Liquefaction," *Geotechnical Earthquake Engineering & Soil Dynamics IV*.

Doar, R.D. and C.G. Kendall (2014). "An Analysis and Comparison of Observed Pleistocene South Carolina (USA) Shoreline Elevations with Predicted Elevations Derived from Marine Oxygen Isotope Stages," *Quaternary Research*, Vol. 82, pp. 164–174.

Eller, J.M. and S.A. Ashford (2011). "Blast-Induced Liquefaction for Earthquake Studies," *Proceedings, 8th International Conference on Urban Earthquake Engineering*, 6 pp.

Gianella, T.N. (2015). "Ground Improvement and Liquefaction Mitigation using Driven Timber Piles," M.S. Thesis, Oregon State University, Corvallis, 506 pp.

Hansbo, S. (1979). "Consolidation of Clay by Bandshaped Prefabricated Drains," *Ground Engineering*, Vol. 12, No. 5, pp. 16–25.

Hayward Baker, Inc. (2014). Mebra-Drain MD-88 Technical Specifications, HB Wick Drains, Centennial, Colo.

Kulhawy, F.H. and P.W. Mayne (1990). *Manual on Estimating Soil Properties for Foundation Design*, No. EPRI-EL-P800, Electric Power Research Institute, Palo Alto, Calif. (USA); Cornell University, Ithaca, N.Y. (USA), Geotechnical Engineering Group.

Lee, K.L. and A. Albaisa (1974). "Earthquake Induced Settlements in Saturated Sands," *Journal of the Geotechnical Engineering Division*, Vol. 100 (GT4), ASCE, New York, N.Y., pp. 387–406.

Mayne, P.W. (2007). *NCHRP Synthesis 368: Cone Penetration Testing*, Transportation Research Board of the National Academies, Washington, D.C., 126 pp.

Pestana, J.M., C.E. Hunt, and R.R. Goughnour (1997). "FEQDrain: A Finite Element Computer Program for the Analysis of the Earthquake Generation and Dissipation of Pore Water Pressure in Layered Sand Deposits with Vertical Drains," Report No. UCB/EERC-97/15, University of California, Berkeley, 88 pp.

PHRI, Port and Harbour Research Institute (1997). "Handbook on Liquefaction Remediation of Reclaimed Land," Balkema, Rotterdam, the Netherlands.

Robertson, P.K. and C.E. Wride (1998). "Evaluating Cyclic Liquefaction Potential Using the Cone Penetration Test," *Canadian Geotechnical Journal*, Vol. 35, No. 3, pp. 442–459.

Rollins, K.M., J. Anderson, A. McCain, and R. Goughnour (2004). "Vertical Composite Drains for Mitigating Liquefaction Hazard," In *Proceedings of the 13th International Offshore and Polar Engineering Conference*, pp. 498–505.

Rollins, K.M., J.D. Lane, E. Dibb, S.A. Ashford, and A.G. Mullins (2005). "Pore Pressure Measurement in Blast-Induced Liquefaction Experiments," *Transportation Research Record: Journal of the Transportation Research Board, No. 1936*, Transportation Research Board of the National Academies, Washington, D.C., pp. 210–220.

Seed, H.B., P.P Martin, and J. Lysmer (1975) *The Generation and Dissipation of Pore Water Pressures During Soil Liquefaction*, Report No. UCB/EERC 75-26, Earthquake Engineering Research Center.

Seed, H.B. and I.M. Idriss (1982). *Ground Motions and Soil Liquefaction During Earthquakes*, Earthquake Engineering Research Institute Monograph MNO-5, 134 pp.

Seed, H.B. K. Tokimatsu, L.F. Harder, and R.M. Chung "Influence of SPT Procedures in Soil Liquefaction Resistance Evaluations," *Journal of Geotechnical Engineering*, Vol. 111, No. 12, pp. 1425–1445.

South Carolina Department of Transportation (SCDOT) (2008). *Geotechnical Design Manual*, South Carolina Geology and Seismicity.

APPENDIX A

NUMERICAL ANALYSES

Table A1. Summary of calibrated input parameters for the control zone using FEQDrain

Layer #	Layer Thickness and Number of Sublayers	Calibrated Parameters
1	2.13 m 7 layers	k_h = 7.3 x 10^{-2} cm/s k_v = 1.8 x 10^{-2} cm/s m_v = 3.3 x 10^{-5} m^2/kN D_r = 0.58, N_L = 20 γ_{sat} = 19.1 kN/m^3, θ = 0.7
2	2.44 m 8 layers	k_h = 1.6 x 10^{-2} cm/s k_v = 1.0 x 10^{-2} cm/s m_v = 2.0 x 10^{-5} m^2/kN D_r = 0.46, N_L = 17 γ_{sat} = 18.4 kN/m^3, θ = 0.8
3	1.22 m 4 layers	k_h = 1.6 x 10^{-2} cm/s k_v = 1.0 x 10^{-2} cm/s m_v = 2.0 x 10^{-5} m^2/kN D_r = 0.30, N_L = 18 γ_{sat} = 17.3 kN/m^3, θ = 0.8
4	3.96 m 13 layers	k_h = 2.4 x 10^{-2} cm/s k_v = 6.1 x 10^{-3} cm/s m_v = 3.3 x 10^{-5} m^2/kN D_r = 0.40, N_L = 16 γ_{sat} = 18.1 kN/m^3, θ = 0.8
5	2.44 m 8 layers	k_h = 2.4 x 10^{-2} cm/s k_v = 6.1 x 10^{-3} cm/s m_v = 3.3 x 10^{-5} m^2/kN D_r = 0.25, N_L = 15 γ_{sat} = 17.3 kN/m^3, θ = 0.8
6	2.44 m 8 layers	k_h = 3.4 x 10^{-2} cm/s k_v = 2.2 x 10^{-2} cm/s m_v = 2.0 x 10^{-5} m^2/kN D_r = 0.90, N_L = 1000 γ_{sat} = 20.7 kN/m^3, θ = 0.5
7	0.61 m 2 layers	k_h = 4.0 x 10^{-4} cm/s k_v = 1.0 x 10^{-6} cm/s m_v = 3.3 x 10^{-5} m^2/kN D_r = 0.41, N_L = 15 γ_{sat} = 18.1 kN/m^3, θ = 0.7

Table A2. Cyclic resistance ratio and number of cycles to induce liquefaction in each layer in the control zone

Depth (m)	Layer No.	Average $N_{1,60}$	Average *FC* (%)	*CRR*	N_L
0 to 2.13	1	8	20.9	0.135	20
2.13 to 4.57	2	14	2.5	0.150	17
4.57 to 5.79	3	7	7.9	0.075	18
5.79 to 9.75	4	17	9.0	0.230	16
9.75 to 12.19	5	11	28.1	0.190	15
12-19 to 14.63	6	47	1.16	N/A	1000
14.63 to 15.24	7	8	40.0	0.160	15

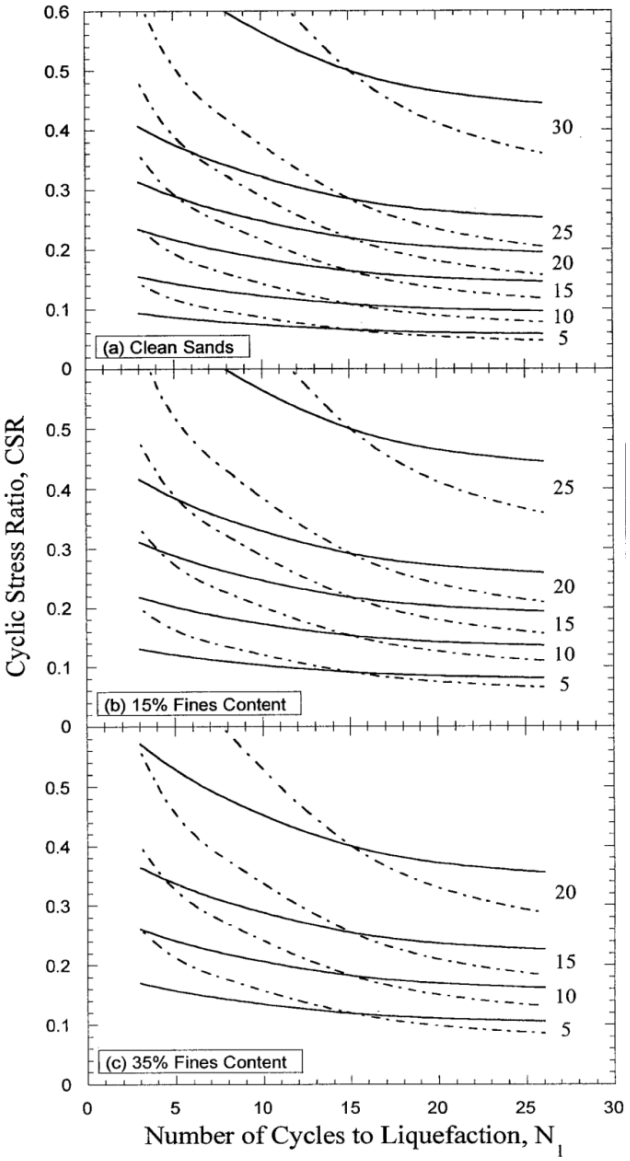

FIGURE A1 Cyclic stress ratio versus corrected penetration resistance for initial triggering liquefaction for varying fines content after Pestana et al. (1997). The dashed lines correspond to magnitude scaling factors recommended in the 1996 NCEER workshop (after Youd and Idriss 1996). Note that this figure provides the *CRR* = the *CSR* required to trigger liquefaction.

Table A3. Summary of calibrated input parameters for the control zone using FEQDrain

Layer No.	Layer Thickness and Number of Sublayers	Calibrated Parameters
1	2.13 m 7 layers	k_h = 7.3 x 10^{-2} cm/s k_v = 1.8 x 10^{-2} cm/s m_v = 3.3 x 10^{-5} m^2/kN D_r = 0.58, N_L = 20 γ_{sat} = 19.1 kN/m^3, θ = 0.7
2	2.44 m 8 layers	k_h = 1.6 x 10^{-2} cm/s k_v = 1.0 x 10^{-2} cm/s m_v = 2.0 x 10^{-5} m^2/kN D_r = 0.46, N_L = 17 γ_{sat} = 18.4 kN/m^3, θ = 0.8
3	1.22 m 4 layers	k_h = 1.6 x 10^{-2} cm/s k_v = 1.0 x 10^{-2} cm/s m_v = 2.0 x 10^{-5} m^2/kN D_r = 0.30, N_L = 18 γ_{sat} = 17.3 kN/m^3, θ = 0.8
4	3.96 m 13 layers	k_h = 2.4 x 10^{-2} cm/s k_v = 6.1 x 10^{-3} cm/s m_v = 3.3 x 10^{-5} m^2/kN D_r = 0.40, N_L = 16 γ_{sat} = 18.1 kN/m^3, θ = 0.8
5	2.44 m 8 layers	k_h = 2.4 x 10^{-2} cm/s k_v = 6.1 x 10^{-3} cm/s m_v = 3.3 x 10^{-5} m^2/kN D_r = 0.25, N_L = 15 γ_{sat} = 17.3 kN/m^3, θ = 0.8
6	2.44 m 8 layers	k_h = 3.4 x 10^{-2} cm/s k_v = 2.2 x 10^{-2} cm/s m_v = 2.0 x 10^{-5} m^2/kN D_r = 0.90, N_L = 1000 γ_{sat} = 20.7 kN/m^3, θ = 0.5
7	0.61 m 2 layers	k_h = 4.0 x 10^{-4} cm/s k_v = 1.0 x 10^{-6} cm/s m_v = 3.3 x 10^{-5} m^2/kN D_r = 0.41, N_L = 15 γ_{sat} = 18.1 kN/m^3, θ = 0.7

Table A4. Cyclic resistance ratio and number of cycles to induce liquefaction for each layer in Zone 1 following installation

Depth (m)	Layer No.	Average $N_{1,60}$	Average *FC*	*CRR*	N_L
0 to 2.13	1	6	21.8	0.12	12
2.13 to 5.18	2	16	10.2	0.20	19
5.18 to 7.92	3	23	7.4	0.27	23
7.92 to 12.19	4	12	18.3	0.19	14
12.19 to 14.63	5	33	1.8	NA	1000
14.63 to 15.24	6	11	31.2	0.19	17

Table A5. Cyclic resistance ratio and number of cycles to induce liquefaction for each layer in Zone 2 following installation

Depth (m)	Layer No.	Average $N_{1,60}$	Average *FC*	*CRR*	N_L
0 to 2.13	1	35	13.9	NA	30
2.13 to 5.18	2	19	5.6	0.21	14
5.18 to 8.53	3	21	8.5	0.24	21
8.53 to 12.49	4	12	14.6	0.18	15
12.49 to 14.63	5	48	1.8	NA	1000
14.63 to 15.24	6	11	34.0	0.19	17

Table A6. Cyclic resistance ratio and number of cycles to induce liquefaction for each layer in Zone 3 following installation

Depth (m)	Layer No.	Average $N_{1,60}$	Average *FC*	*CRR*	N_L
0 to 2.13	1	28	15.0	NA	30
2.13 to 5.18	2	14	8.3	0.17	18
5.18 to 9.14	3	13	6.3	0.15	13
9.14 to 12.49	4	3	21.7	0.08	15
12.49 to 14.63	5	32	1.8	NA	1000
14.63 to 15.24	6	11	31.2	0.19	17

Table A7. Cyclic resistance ratio and number of cycles to induce liquefaction for each layer in Zone 4 following installation

Depth (m)	Layer No.	Average $N_{1,60}$	Average *FC*	*CRR*	N_L
0 to 2.13	1	10	25.1	0.17	16
2.13 to 5.18	2	24	5.8	0.27	15
5.18 to 9.45	3	18	7.4	0.21	18
9.45 to 12.80	4	6	13.1	0.11	14
12.80 to 14.63	5	44	1.8	NA	1000
14.63 to 15.24	6	11	20.9	0.17	14

Table A8. Summary of soil input parameters using FEQDrain for Zone 1 following pile installation

Layer No.	Layer Thickness and Number of Sublayers	Input Parameters
1	2.13 m 7 layers	k_h = 7.3 x 10^{-2} cm/s k_v = 1.8 x 10^{-2} cm/s m_v = 3.3 x 10^{-5} m^2/kN D_r = 0.50, N_L = 12 γ_{sat} = 18.7 kN/m^3, θ = 0.7
2	3.05 m 10 layers	k_h = 1.6 x 10^{-2} cm/s k_v = 1.0 x 10^{-2} cm/s m_v = 2.0 x 10^{-5} m^2/kN D_r = 0.55, N_L = 19 γ_{sat} = 18.9 kN/m^3, θ = 0.7
3	2.74 m 9 layers	k_h = 2.4 x 10^{-2} cm/s k_v = 6.1 x 10^{-3} cm/s m_v = 3.3 x 10^{-5} m^2/kN D_r = 0.58, N_L = 15 γ_{sat} = 19.2 kN/m^3, θ = 0.7
4	4.27 m 14 layers	k_h = 2.4 x 10^{-2} cm/s k_v = 6.1 x 10^{-3} cm/s m_v = 3.3 x 10^{-5} m^2/kN D_r = 0.30, N_L = 14 γ_{sat} = 17.3 kN/m^3, θ = 0.8
5	2.44 m 8 layers	k_h = 3.4 x 10^{-2} cm/s k_v = 2.2 x 10^{-2} cm/s m_v = 2.0 x 10^{-5} m^2/kN D_r = 0.90, N_L = 1000 γ_{sat} = 20.7 kN/m^3, θ = 0.5
6	0.61 m 2 layers	k_h = 4.0 x 10^{-4} cm/s k_v = 1.0 x 10^{-6} cm/s m_v = 3.3 x 10^{-5} m^2/kN D_r = 0.50, N_L = 17 γ_{sat} = 18.7 kN/m^3, θ = 0.7

Table A9. Summary of soil input parameters using FEQDrain for Zone 2 following pile installation

Layer No.	Layer Thickness and Number of Sublayers	Input Parameters
1	2.13 m 7 layers	k_h = 7.3 x 10^{-2} cm/s k_v = 1.8 x 10^{-2} cm/s m_v = 3.3 x 10^{-5} m^2/kN D_r = 0.50, N_L = 30 γ_{sat} = 18.7 kN/m^3, θ = 0.7
2	3.05 m 10 layers	k_h = 1.6 x 10^{-2} cm/s k_v = 1.0 x 10^{-2} cm/s m_v = 2.0 x 10^{-5} m^2/kN D_r = 0.76, N_L = 14 γ_{sat} = 20.1 kN/m^3, θ = 0.7
3	3.35 m 11 layers	k_h = 2.4 x 10^{-2} cm/s k_v = 6.1 x 10^{-3} cm/s m_v = 3.3 x 10^{-5} m^2/kN D_r = 0.83, N_L = 21 γ_{sat} = 20.4 kN/m^3, θ = 0.7
4	3.96 m 13 layers	k_h = 2.4 x 10^{-2} cm/s k_v = 6.1 x 10^{-3} cm/s m_v = 3.3 x 10^{-5} m^2/kN D_r = 0.57, N_L = 15 γ_{sat} = 19.2 kN/m^3, θ = 0.7
5	2.13 m 7 layers	k_h = 3.4 x 10^{-2} cm/s k_v = 2.2 x 10^{-2} cm/s m_v = 2.0 x 10^{-5} m^2/kN D_r = 0.90, N_L = 1000 γ_{sat} = 20.7 kN/m^3, θ = 0.5
6	0.61 m 2 layers	k_h = 4.0 x 10^{-4} cm/s k_v = 1.0 x 10^{-6} cm/s m_v = 3.3 x 10^{-5} m^2/kN D_r = 0.50, N_L = 17 γ_{sat} = 18.7 kN/m^3, θ = 0.7

Table A10. Summary of soil input parameters using FEQDrain for Zone 3 following pile installation

Layer No.	Layer Thickness and Number of Sublayers	Input Parameters
1	2.13 m 7 layers	k_h = 7.3 x 10^{-2} cm/s k_v = 1.8 x 10^{-2} cm/s m_v = 3.3 x 10^{-5} m^2/kN D_r = 0.50, N_L = 30 γ_{sat} = 18.7 kN/m^3, θ = 0.7
2	3.05 m 10 layers	k_h = 1.6 x 10^{-2} cm/s k_v = 1.0 x 10^{-2} cm/s m_v = 2.0 x 10^{-5} m^2/kN D_r = 0.57, N_L = 18 γ_{sat} = 19.2 kN/m^3, θ = 0.7
3	3.96 m 13 layers	k_h = 2.4 x 10^{-2} cm/s k_v = 6.1 x 10^{-3} cm/s m_v = 3.3 x 10^{-5} m^2/kN D_r = 0.60, N_L = 13 γ_{sat} = 19.3 kN/m^3, θ = 0.7
4	3.35 m 11 layers	k_h = 2.4 x 10^{-2} cm/s k_v = 6.1 x 10^{-3} cm/s m_v = 3.3 x 10^{-5} m^2/kN D_r = 0.28, N_L = 15 γ_{sat} = 17.3 kN/m^3, θ = 0.8
5	2.13 m 7 layers	k_h = 3.4 x 10^{-2} cm/s k_v = 2.2 x 10^{-2} cm/s m_v = 2.0 x 10^{-5} m^2/kN D_r = 0.90, N_L = 1000 γ_{sat} = 20.7 kN/m^3, θ = 0.5
6	0.61 m 2 layers	k_h = 4.0 x 10^{-4} cm/s k_v = 1.0 x 10^{-6} cm/s m_v = 3.3 x 10^{-5} m^2/kN D_r = 0.50, N_L = 17 γ_{sat} = 18.7 kN/m^3, θ = 0.7

Table A11. Summary of soil input parameters using FEQDrain for Zone 4 following pile installation

Layer No.	Layer Thickness and Number of Sublayers	Input Parameters
1	2.13 m 7 layers	k_h = 7.3 x 10^{-2} cm/s k_v = 1.8 x 10^{-2} cm/s m_v = 3.3 x 10^{-5} m^2/kN D_r = 0.60, N_L = 16 γ_{sat} = 19.3 kN/m^3, θ = 0.7
2	3.05 m 10 layers	k_h = 1.6 x 10^{-2} cm/s k_v = 1.0 x 10^{-2} cm/s m_v = 2.0 x 10^{-5} m^2/kN D_r = 0.70, N_L = 15 γ_{sat} = 19.8 kN/m^3, θ = 0.7
3	4.27 m 14 layers	k_h = 2.4 x 10^{-2} cm/s k_v = 6.1 x 10^{-3} cm/s m_v = 3.3 x 10^{-5} m^2/kN D_r = 0.65, N_L = 18 γ_{sat} = 19.6 kN/m^3, θ = 0.7
4	3.35 m 11 layers	k_h = 2.4 x 10^{-2} cm/s k_v = 6.1 x 10^{-3} cm/s m_v = 3.3 x 10^{-5} m^2/kN D_r = 0.45, N_L = 14 γ_{sat} = 18.4 kN/m^3, θ = 0.8
5	1.83 m 6 layers	k_h = 3.4 x 10^{-2} cm/s k_v = 2.2 x 10^{-2} cm/s m_v = 2.0 x 10^{-5} m^2/kN D_r = 0.90, N_L = 1000 γ_{sat} = 20.7 kN/m^3, θ = 0.5
6	0.61 m 2 layers	k_h = 4.0 x 10^{-4} cm/s k_v = 1.0 x 10^{-6} cm/s m_v = 3.3 x 10^{-5} m^2/kN D_r = 0.50, N_L = 14 γ_{sat} = 18.7 kN/m^3, θ = 0.7